Electromagnetic Scattering by Metallic Structures with Edges Excited by Multiple Plane Waves

by

BAKER B. AL-BAHRI
B.A. University of Baghdad, 1996
M.S. University of Baghdad, 2001
Ph.D. Al-Nahrain University, 2006
M.S. University of Illinois at Chicago, 2016

THESIS

Submitted as partial fulfillment of the requirements
for the degree of Doctor of Philosophy in Electrical and Computer Engineering
in the Graduate College of the
University of Illinois at Chicago, 2021

Chicago, Illinois

Defense Committee:

Piergiorgio L. E. Uslenghi, Chair and Advisor
Pai-Yan Chen
Danilo Erricolo
Besma Smida
Marco D. Poort, Google

To my small family, my wife “ZAINAB” and my six years daughter “LARA”, I dedicate this work. Without them it would never have been accomplished.

ACKNOWLEDGMENTS

Praise be to GOD; The Most Beneficent, The Most Merciful.

I would like to thank my advisor; Professor Piergiorgio L. E. Uslenghi, who gave me unlimited help, support and time during the research. Also, I would like to express my appreciation to the other members of my thesis committee, Professors: Pai-Yan Chen, Danilo Erricolo, Besma Smida, and to Dr. Marco D. Poort for their unwavering support and assistance to me to accomplish my research in the best form.

My special thanks go to my wife Zainab, who encourages me all the time and gives me all the support not only in this work, but in my entire life. My deep thanks to my parents, I really appreciate everything they have done for me. My thanks to my little daughter Lara for being patient, when I was busy in the study and did not give her enough attention.

My thanks goes to our best friends Carolyn Williams and Michael Williams, Lynn Thomas, and Diane Highland. Also, I would like to thank Tina and Evelyn from ECE students affairs. Finally, my thanks to all people who helped me to finish this work.

BA

TABLE OF CONTENTS

TABLE OF CONTENTS (Continued)

CHAPTER **PAGE**

LIST OF FIGURES

LIST OF FIGURES (Continued)

FIGURE **PAGE**

LIST OF FIGURES (Continued)

FIGURE **PAGE**

SUMMARY

The electromagnetic scattering by complex structures is important in a variety of applications: cellular communications; propagation in indoor and outdoor environments; vehicular technology; microwave components and devices; antennas and arrays; radar signatures of ground vehicles, ships, aircraft, missiles and satellites; detection of buried objects; security screening; implanted health-care devices. The scattering behavior of these structures can be studied by analytical, numerical and experimental methods. Among the analytical methods, many results have been obtained via exact solutions or approximate techniques such as low-frequency and high-frequency methods. Exact solutions, also called canonical solutions, are available only for relatively simple geometries, materials, and primary sources; however, they are very important because they provide information on the behavior of more complicated structures and because they constitute valuable tools for the validation of computer solvers.

Many structures of interest contain sharp metallic edges, which constitute an important source of scattered fields that are often unwanted but difficult to blunt for many reasons such as the shape of the metallic structure, the nature of the incident wave, ...etc. This dissertation presents geometrical optics solutions that are exact solutions for the considered boundary-value problems. This goal is achieved by selecting the number, polarization, amplitude, phase and direction of incidence of the primary plane waves in such a way that the edges of the metallic structures do not scatter, that the boundary conditions on the surfaces of these structures are satisfied, and that there are no field discontinuities across optical boundaries. Additionally,

certain relations among the angle of incidence, wavelength, dimensions of the metallic structure and spacing between the structures (if more than one structure exist) must be satisfied. The resulting exact total field is the sum of the incident fields and sometimes it generates mode(s) propagates in certain directions and/or it consists of standing waves in the space surrounding the structures. It is proven in this work that for the metal structures with strips and right-angle wedges the exact geometrical optics solutions are possible under incidence by multiple plane waves, if certain important conditions are satisfied.

This dissertation proposes a method, we call it "Grid Method", which can be introduced as a general procedure developed for obtaining exact geometrical optics (GO) scattering solutions under incidence by multiple primary or imaged plane waves impinging upon a two-dimensional structure consisting of simply or multiply connected perfect electric conductor (PEC) strips either parallel or perpendicular to one another. The grid method provides all the conditions that must be satisfied to assure the existence of the GO solution to the boundary-value problem. The key feature behind applying the grid method is that the edges of the metallic structure will not scatter, which means that the GO solution represents the exact solution to the boundary-value problem. For some structures, we consider the case of a single incident plane wave and find the solution to scattering by this wave using the Wiener-Hopf theoretic method. Then, the obtained solutions by considering each single incident wave individually, are added to get the total solution to the boundary-value problem, which is the same as the GO solution developed by using the grid method.

Next, the two-dimensional problems of scattering by several metallic structures with strips and

right-angle wedges such as metallic grating, prism, rectangular cylinders ...etc are developed based on the proposed grid method. All the required conditions to guarantee the existence of the GO solution are stated and applied.

The two-dimensional results obtained by applying the grid method are generalized to the three-dimensional solutions by considering the oblique incidence of the primary waves with respect to the z-axis, when the metallic structures are perpendicularly truncated by a ground metal plate.

Numerical results for the surface current densities on the surface of the metallic structures and the truncating plane are shown and discussed. The analysis is carried out in the phasor domain with a time-dependence factor $\exp(+j\omega t)$ omitted throughout.

The importance of the proposed grid method is twofold: it provides novel canonical solutions to scattering problems, and it may be a helpful tool in validating both complicated analytical solutions and numerical solutions obtained via commercially available computer solvers.

CHAPTER 1

INTRODUCTION

The electromagnetic scattering by complex structures has a wide range of applications such as wireless communications; microwave components and devices; antennas and arrays; radar systems, satellites; detection of buried objects; security screening; health-care devices and many more.

The solution to the scattering problem can be found by different methods. The exact solution to the boundary-value problem is the best solution since it has no numerical approximation. Sometimes, it is difficult to obtain the exact solution to the boundary-value problem because of complicated geometry of the scattering structures.

This study presents a method to eliminate the scattering by edges in the metallic structures with strips and right-angle wedges, which leads to make the GO solution the exact solution to the boundary-value problem. In this thesis, the solutions to 2-D and 3-D scattering problems by several metallic structures with strips and right-angle wedges are developed. In this chapter, a historical background about the scattering by metallic structures with sharp edges is presented as a starting point in this work. Also, the thesis statement and the organization of this document are provided.

1.1 Historical Background

Many structures of interest contain sharp metallic edges, which are considered an effective source of scattered fields that are often unwanted, but difficult to blunt. Hence, the study of scattering by metallic wedges, and in particular of the metallic half-plane, has an illustrious history, beginning with the works of Sommerfeld (1) who obtained the exact and closed-form solution to the scattering of a plane wave by a metallic half-plane, and of MacDonald (2) who derived the exact solution to the scattering of a plane wave or a line source by a metallic wedge of arbitrary aperture angle as an infinite series of circular-cylinder wavefunctions.

The electromagnetic scattering by infinite number of parallel metallic half-planes under a single plane wave incident perpendicularly to the edges was solved analytically for the E-polarization in (3) and for the H-polarization in (4). The same 2-D problem was investigated again with more details by Whitehead in (5). Heins in (6) investigated the field outside the parallel half-planes. The 2-D problem of the scattering at the end of open waveguide was investigated and solved in (7). The electromagnetic scattering by two parallel half-planes excited by single plane wave incident perpendicularly to the edges was solved analytically using the Wiener-Hopf function theoretic method in (8; 9). The same problem was solved with more details about applying the Wiener-Hopf function theoretic method in (10) and (11). An analytical solution to the problem of electromagnetic scattering by an array of parallel metallic half-planes perpendicularly truncated by a metal plane was presented in (12; 13) where the 2-D solution presented in (3) and (4) is generalized to the case of an arbitrarily polarized plane wave that is obliquely incident upon the edges of the half-planes.

The 2-D electromagnetic scattering problem solved previously in (8) and (9) was generalized to the 3-D problem by considering an arbitrarily polarized plane wave obliquely incident on the edges of the truncated half-planes in (14); this was achieved by following the general procedure detailed in (15). The scattering by an infinite array of semi-infinite thick plates were investigated in (16) and (17).

Uslenghi in (18) showed that under two symmetrical incident plane waves, which fall upon the edge of half-plane, the edge does not scatter and the GO solution represents the exact solution to the boundary-value problem. This can be verified by developing Sommerfels's solution for each incident wave separately, which will be in term of Fresnel integrals (19), then adding the results and using some properties of the Fresnel integral; it can be shown that the edge does not scatter and that the field everywhere is the summation of the two incident plane waves. Structures with metallic wedges that are amenable to simple, exact solutions via geometrical optics and contain isorefractive materials or rely on Brewster total transmission have been obtained by Uslenghi in (20; 21; 22; 23; 24). The only presently available exact GO solution to the scattering of a plane wave by a wedge involves a right-angle DNG metamaterial wedge (25). The exact geometrical optics scattering by a truncated rectangular metal trench was presented (26). An exact GO solution to the scattering of a plane wave by a metallic wedge is not possible; however, such a solution may exist when the wedge is excited by more than one plane wave (27; 28; 29; 30; 31; 32).

This dissertation proposes a method, which we call "Grid method" (33), which can be used to develop GO solutions to the scattering by metal structures with strips and right-angle wedges

under multiple plane wave excitation. The grid method is presented and discussed in chapter 2, and many specific applications are presented in chapter 3. The obtained GO solutions represent the exact solution to the boundary-value problem.

The proposed grid method is applied to find the exact 2-D solution to the scattering by different metal structures such as arrays of infinite (or finite) equally (or unequally) spaced parallel half-planes, arrays of infinite (or finite) equally spaced thick half-planes, metal gratings which consist of a finite (or infinite) number of grooves and ridges of rectangular cross-section on a metal plate (31), and arrays of pillars of rectangular cross-section.

The obtained 2-D GO solution is generalized to 3-D solution by considering an arbitrarily polarized plane wave that is obliquely incident on the edges of the metallic structure when the latter is perpendicularly truncated by a ground metal plate, following the procedure in (15). All the relations and conditions that are required to ensure the existence of the 2-D and 3-D GO solutions will be derived. Particular attention will be devoted to the surface current densities on the metal structures. The analysis is carried out in the phasor domain with a time-dependence factor $\exp(+j\omega t)$ omitted throughout.

1.2 Thesis Statement

This dissertation investigates and develops GO solutions to the electromagnetic scattering by metal structures with strips and right-angle wedges. It is proven that the obtained GO solutions represent the exact solution to the electromagnetic boundary-value problem.
A general procedure called "Grid Method" (33) is developed and used to obtain the GO solution

to the boundary-value problem; it assures that this GO solution represents the exact solution to the boundary-value problem under multiple plane waves excitation. Two-dimensional solutions to the electromagnetic scattering by several structures are developed using the grid method, then these 2-D solutions are generalized to the 3-D solutions. Numerical results for the surface current densities on the surface of these metallic structures are developed, shown and discussed.

1.3 Outline of Document

This document starts with reviewing historical background of the scattering problem by metallic structures containing sharp edges, in chapter 1. The survey includes the scattering by a half-plane, a pair of half-planes, arrays of half-planes, wedges and some other similar metallic structures.

In chapter 2, the grid method (33) is proposed and developed. The grid method is a general procedure that can be used to obtain the GO solution to the electromagnetic scattering by metallic structures contains strips and right-angle wedges under multiple plane waves excitation. Several conditions and relations related to the dimensions of the metal structures, spacing between the components of the metal structure, wavelength, incidence angle and polarization of the incident plane waves are developed and provided in chapter 2 for the 2-D solutions and in chapter 3 for the 3-D solutions. The general steps to form and apply the grid method are explained at the end of chapter 2.

In chapter 3, the proposed grid method is used to develop the exact solution to the boundary-value problem for several structures such as array of half-planes, array of thick half-planes,

gratings, rectangular cylinders, ...etc. The problems are solved in two steps. First, the 2-D solution to the scattering problem under multiple plane waves excitation is developed using the grid method, with developing and stating all the conditions that must be satisfied in order to make the edges of these structures not scatter; therefore, the GO solution represents the exact solution to the boundary-value problem. In the second step, the obtained 2-D solution is generalized to the 3-D solution based on the procedure in (15). Also, numerical results for the current density on the surface of the metallic structures are shown and discussed.

Finally, in chapter 4 the main conclusions based on the analysis and results are presented and some future extensions that can be built on the results in this thesis are proposed.

CHAPTER 2

GRID METHOD

2.1 Introduction

Electromagnetic scattering by metallic structures with sharp edges such as wedges, gratings, rectangular pillars, ...etc is important in a variety of practical applications. The main difficulty associated with such structures from this geometry is the presence of the edge singularities, which make the edges scatter. This can be a challenge to be solved by computer solvers (34). While it is often desirable to minimize the scattering by edges, this objective can not be achieved under incidence by a single plane wave, but may be possible when several plane waves with the same frequency, each having an appropriate amplitude, phase, polarization and direction of incidence, are impinging upon the metallic structure. In such instances, the linear, homogeneous and isotropic space (e.g., air) surrounding the structure is filled with standing plane waves, and the edges of the metallic structure do not scatter; therefore, the geometrical optics solution is the exact solution to the boundary-value problem. Such a solution has been obtained for a class of metallic wedges in (32), and is valid for any frequency of the incident waves. Because the metallic wedges under consideration do not have any characteristic length, no restrictions are applied. In more complex metallic structures, which have characteristic lengths, additional restrictions involving characteristic lengths of the metallic structures, wavelength, polarization, number of incident plane waves and angles of incidence may have to be imposed on the solution

in order to make the edges of these metallic structures not scatter and hence the GO solutions are the exact solutions to the problem, as is the case in (26; 29; 30; 31). A general procedure to obtain the exact GO solutions to the scattering by specific metallic structures with strips and right-angle wedges such as metallic gratings, trenches, ridges, ...etc under multiple plane waves excitation is presented in (33).

In this chapter, the grid method is developed to obtain the two-dimensional GO solutions to the electromagnetic scattering by specific metallic structures. These structures consist of simply or multiply connected bodies whose boundaries are any number of planar perfect electric conducting strips that are parallel to one another and either parallel or perpendicular to the same plane. It is shown that, under incidence by four appropriate plane waves with satisfying certain relations among the wavelength, the angle of incidence, and the dimensions of the metallic structures, the edges of these structures do not scatter, that the boundary conditions on the surfaces of the metallic structures are satisfied and that there are no field discontinuities across optical boundaries, which make the GO solution the exact solution to the scattering problem by these structures. The analysis is conducted in the phasor domain with a time-dependence factor $\exp(+\mathrm{j}\omega\mathrm{t})$ omitted throughout.

The PEC strips are of infinite length and are oriented in the $z-$direction of a rectangular coordinate system (x, y, z). Each strip occupies a portion of either the (x, z) plane or the (y, z) plane, and is either isolated or in contact at right angle with a neighboring strip or two. Thus, at any plane $z = constant$, the same 2-D structure is obtained.

The first step in the analysis (section 2.2) consists in considering four plane waves, which create a uniform rectangular grid of standing waves. Each element of the grid is a rectangle. The total electric field due to the four waves is perpendicular to the sides of the rectangle and is zero at its vertices, which means that one or more faces of the rectangle can be metallized without disturbing the field, and that the metal edges do not scatter. This result is possible if the periods of the grid in the $x-$ and $y-$directions, the wavelength, and the angles of incidence of the primary waves satisfy a couple of relations, which are derived and discussed in detail in this chapter. The analysis is performed for the two cases E-polarization (electric field parallel to the $z-$axis) and H-polarization (magnetic field parallel to the $z-$axis).

If the penetrable space around the metal structure occupies only one, or two, or three quadrants, then the number of primary plane waves may be reduced to one, two, or three, respectively. The remaining waves needed to form the grid are supplied by the images of the incident waves into the PEC walls of the structure. Several examples are given and discussed in sections 2.3, 2.4 and 2.5 about one-quadrant, two-quadrant, and three-quadrant metallic structures, respectively. Some structures requiring four primary waves are discussed in section 2.6. The general steps to form the grid and apply the grid method are outlined at the end in section 2.7.

2.2 Grid Formulation

Four incident plane waves under certain conditions (described herein) are required to assure the existence of the exact GO solutions. The electric field amplitude of each of the incident plane

waves is normalized to 1 V/m. The four incident plane waves in two-dimensional geometry are given in Equation 2.1 to Equation 2.4 for the E-polarization. The direction of propagation of the four incident plane waves $E_z^{(e)i1}, E_z^{(e)i2}, E_z^{(e)i3}$ and $E_z^{(e)i4}$ makes an angle φ_0, $-\varphi_0$, $\pi - \varphi_0$ and $\pi + \varphi_0$ with the $x-$axis, respectively.

$$E_z^{(e)i1} = e^{jk(x\cos\varphi_0 + y\sin\varphi_0)} = e^{jk\rho\cos(\varphi-\varphi_0)} \tag{2.1}$$

$$E_z^{(e)i2} = -e^{jk(x\cos\varphi_0 - y\sin\varphi_0)} = -e^{jk\rho\cos(\varphi+\varphi_0)} \tag{2.2}$$

$$E_z^{(e)i3} = -e^{-jk(x\cos\varphi_0 - y\sin\varphi_0)} = -e^{-jk\rho\cos(\varphi+\varphi_0)} \tag{2.3}$$

$$E_z^{(e)i4} = e^{-jk(x\cos\varphi_0 + y\sin\varphi_0)} = e^{-jk\rho\cos(\varphi-\varphi_0)} \tag{2.4}$$

where $k = 2\pi/\lambda$ is the wavenumber, and $0 \leq \varphi_0 \leq \pi/2$.

The related magnetic fields follow from Maxwell's equations. Consequently, the total incident field is given in Equation 2.5 to Equation 2.7

$$\begin{aligned} E_z^{(e)t} &= \sum_{j=1}^{4} E_z^{(e)ij} \\ &= 2\left\{\cos[k\rho\cos(\varphi-\varphi_0)] - \cos[k\rho\cos(\varphi+\varphi_0)]\right\} \\ &= 2[\cos(k\rho\cos\varphi\cos\varphi_0 + k\rho\sin\varphi\sin\varphi_0) - \cos(k\rho\cos\varphi\cos\varphi_0 - k\rho\sin\varphi\sin\varphi_0)] \\ &= 2[\cos(k_x x + k_y y) - \cos(k_x x - k_y y)] \\ &= -4\sin(k_x x)\sin(k_y y) = U(x,y;k) \end{aligned} \tag{2.5}$$

$$H_x^{(e)t} = -4jY \sin\varphi_0 \sin(k_x x) \cos(k_y y) \tag{2.6}$$

$$H_y^{(e)t} = 4jY \cos\varphi_0 \cos(k_x x) \sin(k_y y) \tag{2.7}$$

where $U(x, y; k)$ is the total solution to the 2-D problem, which will be used in chapter 3 to obtain the 3-D solution to the boundary-value problem, $Y = 1/Z$ is the intrinsic admittance of the medium surrounding the PEC structure, Z is the intrinsic impedance of the medium, k_x and k_y are given in Equation 2.8 and Equation 2.9

$$k_x = k\cos\varphi_0 \tag{2.8}$$

$$k_y = k\sin\varphi_0 \tag{2.9}$$

$$k^2 = k_x^2 + k_y^2. \tag{2.10}$$

If the conditions

$$k_x a = ka\cos\varphi_0 = m\pi, \qquad (m = 0, 1, 2, ...) \tag{2.11}$$

$$k_y b = kb\sin\varphi_0 = n\pi, \qquad (n = 0, 1, 2, ...) \tag{2.12}$$

with m and n non-negative integers are imposed, it follows that

$$E_z^{(e)t}|_{x=ha} = E_z^{(e)t}|_{y=hb} = 0 \tag{2.13}$$

where $h = 0, \pm 1, \pm 2, ...$ is any integer. The entire space is filled with standing waves in the $x-$ and $y-$directions, forming a grid composed of equal rectangles of dimension a in the $x-$direction and b in the $y-$direction. The electric field is perpendicular to the boundaries of all rectangles and is zero at the vertices. Consequently, PEC strips can be inserted at any of the grid boundaries without disturbing the field distribution and the GO solutions are the exact solutions to the scattering problem since the edges of the metallic structure do not scatter.

A similar analysis may be performed for H-polarization (magnetic field parallel to the $z-$axis). The 2-D magnetic field of the four incident plane waves is

$$H_z^{(h)i1} = Ye^{jk(x\cos\varphi_0 + y\sin\varphi_0)} = Ye^{jk\rho\cos(\varphi-\varphi_0)} \tag{2.14}$$

$$H_z^{(h)i2} = Ye^{jk(x\cos\varphi_0 - y\sin\varphi_0)} = Ye^{jk\rho\cos(\varphi+\varphi_0)} \tag{2.15}$$

$$H_z^{(h)i3} = Ye^{-jk(x\cos\varphi_0 - y\sin\varphi_0)} = Ye^{-jk\rho\cos(\varphi+\varphi_0)} \tag{2.16}$$

$$H_z^{(h)i4} = Ye^{-jk(x\cos\varphi_0 + y\sin\varphi_0)} = Ye^{-jk\rho\cos(\varphi-\varphi_0)} \tag{2.17}$$

and the total incident field is given in Equation 2.18 to Equation 2.20

$$\begin{aligned} H_z^{(h)t} &= \sum_{j=1}^{4} H_z^{(h)ij} \\ &= 2Y\left\{\cos[k\rho\cos(\varphi-\varphi_0)]+\cos[k\rho\cos(\varphi+\varphi_0)]\right\} \\ &= 2Y\left[\cos(k\rho\cos\varphi\cos\varphi_0+k\rho\sin\varphi\sin\varphi_0)+\cos(k\rho\cos\varphi\cos\varphi_0-k\rho\sin\varphi\sin\varphi_0)\right] \\ &= 2Y\left[\cos(k_x x+k_y y)+\cos(k_x x-k_y y)\right] \\ &= 4Y\cos(k_x x)\cos(k_y y)=U(x,y;k) \end{aligned} \tag{2.18}$$

$$E_x^{(h)t} = 4j\sin\varphi_0\cos\left(k_x x\right)\sin\left(k_y y\right) \tag{2.19}$$

$$E_y^{(h)t} = -4jY\cos\varphi_0\sin\left(k_x x\right)\cos\left(k_y y\right) \tag{2.20}$$

Under conditions Equation 2.11 and Equation 2.12 we have that

$$E_x^{(h)t}|_{y=hb} = E_y^{(h)t}|_{x=ha} = 0 \tag{2.21}$$

where $h = 0, \pm1, \pm2, ...$ is any integer. As for the case of E-polarization, the electric field is perpendicular to the boundaries of all rectangles in the grid, hence any boundary can be metallized without disturbing the field. A sketch of the grid and the four incident waves in any plane $z = constant$ is shown in Figure 1.

From the fundamental conditions in Equation 2.11 and Equation 2.12

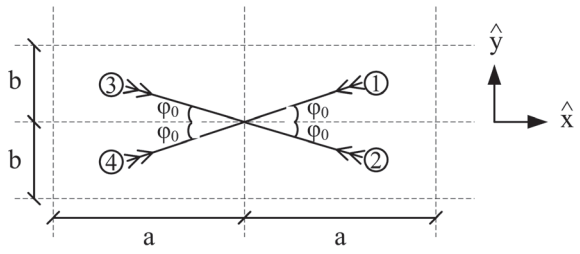

Figure 1. Grid and incident waves.

$$\cos\varphi_0 = m\left(\frac{\pi}{ka}\right) \tag{2.22}$$

$$\sin\varphi_0 = n\left(\frac{\pi}{kb}\right) \tag{2.23}$$

$$\tan\varphi_0 = \frac{na}{mb} \tag{2.24}$$

thus, for given a and b, the incidence angle φ_0 depends on the ratio n/m as shown in Equation 2.24, whereas the wavelength depends on both m and n as shown in Equation 2.25

$$\lambda = \frac{2}{\sqrt{\left(\frac{m}{a}\right)^2 + \left(\frac{n}{b}\right)^2}} \tag{2.25}$$

$$k = \pi\sqrt{\left(\frac{m}{a}\right)^2 + \left(\frac{n}{b}\right)^2} \tag{2.26}$$

Note that Equation 2.11 and Equation 2.12 require that

$$\lambda \leq 2a \quad , \quad \lambda \leq 2b \tag{2.27}$$

respectively, or equivalently the conditions in Equation 2.28 and Equation 2.29 can be obtained

$$f \geq \frac{c}{2a} \quad , \quad f \geq \frac{c}{2b} \tag{2.28}$$

$$m_{max} \leq \frac{2a}{\lambda} \quad , \quad n_{max} \leq \frac{2b}{\lambda} \tag{2.29}$$

where f is the frequency of the incident waves and c is the velocity of the light in the free space. Hence, for given a and b, an exact GO solution is possible only at sufficiently high frequencies. Furthermore, observe that φ_0 and λ are unchanged if a is replaced by a multiple integer of a and b is replaced by a multiple integer of b, provided that m and n are multiplied by those same multiple integers, respectively.

All widths of the metal strips in the $x-$direction must be multiples of a basic-length a, and all widths of metal strips in the $y-$direction must be multiples of a basic-length b, as conditions for the construction of the grid and the existence of GO solutions. Thus, the choice of a and b is not unique; however, it is desirable to select a and b as large as possible in order to lower the minimum value of frequency for which GO solutions are possible based on Equation 2.28.

It is important to note that, there are more than one possible value for the angle of incidence φ_0, basically, it depends on the wavelength λ, the dimensions of the grid or basic-lengths (a and b), and the values of the integers (m and n), these possible values of the angle of incidence φ_0 are computed as follows:

If $a \leq b$ and $m\frac{\lambda}{2} < a < (m+1)\frac{\lambda}{2}$,

then there are m possible values of φ_0 given by

$$\varphi_{0i} = \arccos\left(\frac{i\lambda}{2a}\right), \qquad i = 1, 2, ..., m \tag{2.30}$$

else $a > b$ and $n\frac{\lambda}{2} < b < (n+1)\frac{\lambda}{2}$,

then there are n possible values of φ_0 given by

$$\varphi_{0i} = \arcsin\left(\frac{i\lambda}{2b}\right), \qquad i = 1, 2, ..., n \tag{2.31}$$

where m and n are the integers that are used in Equation 2.11 and Equation 2.12.

Conditions Equation 2.11 and Equation 2.12 are sufficient, but may not be necessary, depending on the geometry of the metallic structure. For example, consider the case of any finite number of metallic strips of arbitrary widths and spacings, but contained in the same plane $y = constant$. Only two incident plane waves (either 1 and 2, or 3 and 4 in Figure 1) that are the image of each other with respect to the plane containing the strips, are needed to satisfy the boundary conditions. Both conditions Equation 2.11 and Equation 2.12 are not needed, and no restrictions need to be imposed on φ_0 and λ for an exact GO solution to exist. If the metallic strips of arbitrary widths and spacings become semi-infinite half-planes and are arranged vertically (i.e. parallel to the $y-$axis) so that one end of each half-plane in the $y = 0$ and the half-planes extend in the negative $y-$axis, then two incident waves (1 and 3) in Figure 1 are required, in addition condition Equation 2.11 must be satisfied to assure the existence of

an exact GO solution. There are innumerable structures that can be analyzed via the grid developed herein; some of them are shown as examples in the following sections.

2.3 One-Quadrant Structures

If the metallic structure, with or without ridges and trenches, occupies the entire half-planes $(x \geq 0, y = 0)$ and $(x = 0, y \geq 0)$ without gaps, then the penetrable medium in contact with the structure occupies only the first quadrant $(x > 0, y > 0)$ of space, plus eventual trenches of finite depth. We refer to such structures as one-quadrant structures for which only the primary wave 1 of Figure 1 is needed, the other three waves in Figure 1 being reflections of wave 1 on the metal walls.

The simplest structure of this type is the dihedral reflector illustrated in Figure 2, that has no characteristic lengths, as its sides extend to infinity and neither step nor trench exist. For such structure neither condition Equation 2.11 nor Equation 2.12 apply; therefore, no restrictions on φ_0 and λ for an exact GO solution to exist.

If either a rectangular step or trench is inserted at the reflector's corner, then characteristic lengths are introduced in the metallic structure and conditions Equation 2.11 and/or Equation 2.12 apply; a suitable choice of the basic-lengths a and b is shown in Figure 3, with the grid boundaries shown as broken lines.

If the parameter a tends to zero or to infinity, or the parameter b tends to zero, then both step and trench in Figure 3 vanish and one reverts to the simple dihedral reflector shown in Figure 2.

If b tends to infinity, the step belongs to a two-quadrant structure since the penetrable medium

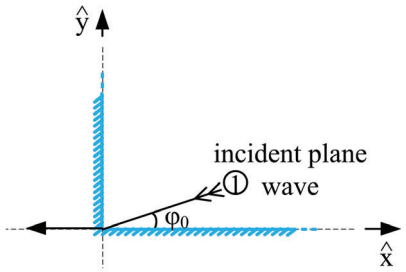

Figure 2. Simple dihedral reflector.

in contact with the structure occupies the first and the fourth quadrants ($x \geq 0, -\infty \leq y \leq +\infty$) of space, which is covered in section 2.4, but the trench becomes a parallel-plate waveguide of semi-infinite length, and the field reflected at the bottom of the trench becomes a mode propagating in the positive $y-$direction inside the guide. For both step and trench structures, only condition Equation 2.11 is needed when b goes to infinity, the incidence angle φ_0 is given by Equation 2.22, and the wavelength of the incident wave must satisfy the condition $\lambda \leq 2a$.

As another example, consider a dihedral reflector whose faces consist of uniform arrays of square ridges and trenches of equal width and depth, as shown in Figure 4. The grid consists of squares of size a, the incidence angle φ_0 is given by $\varphi_0 = \arctan(n/m)$, and the wavelength is $\lambda = 2a/\sqrt{m^2 + n^2}$.

2.4 Two-Quadrant Structures

If the PEC structure, with ridges and trenches of finite height, occupies the entire plane $y = 0$, only the primary waves 1 and 3 of Figure 1 are needed for the possible existence of exact

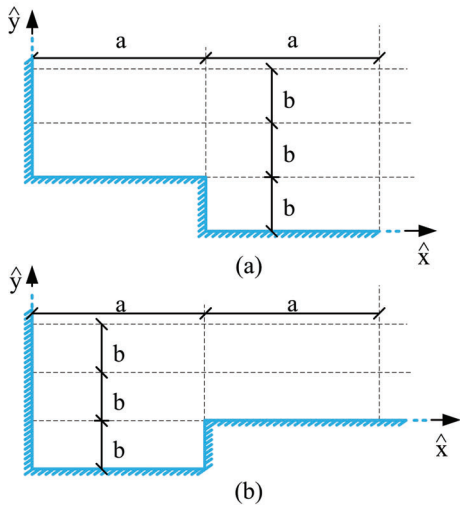

Figure 3. (a) Step and (b) trench in a dihedral reflector.

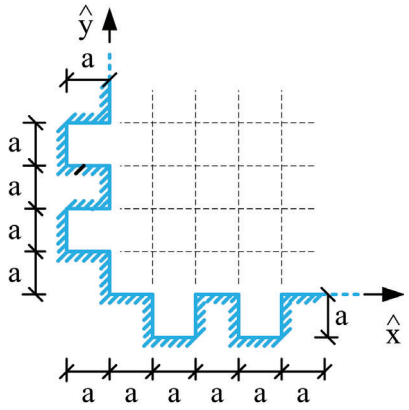

Figure 4. Corrugated dihedral reflector.

GO solutions, the other two waves 2 and 4 being reflections of 1 and 3 into the metal plane. The simplest such two-quadrant structures are the step in a metal plane and the strip perpendicular to a metal plane, both of height b as shown in Figure 5; for these structures only condition Equation 2.12 is needed since there is only one characteristic length in the vertical axis in the metallic structure. There are n possible values for the incidence angle φ_0, which are given in Equation 2.31, where n is the integer that is used in Equation 2.12. The wavelength must satisfy the condition $\lambda \leq 2b$. The scattering of a simple plane wave incident at an arbitrary angle on the strip of Figure 5 has been solved exactly in terms of an infinite series of elliptic-cylinder wavefunctions (35); by combining two such solutions and imposing condition Equation 2.12 it can be verified that an exact GO solution is obtained.

Some other simple two-quadrant structures that require conditions Equation 2.11 and Equation 2.12 such as a rectangular trench or ridge in a metal plane as shown in Figure 6(a) and (b), respectively, or a strip on a metal plane shown in Figure 6(c), where characteristic lengths exist in these structures in the horizontal and vertical axis. Also, both wavelength conditions in Equation 2.27 must be satisfied. There are more than one possible value for the incidence angle φ_0, which are given in Equation 2.30 if $a \leq b$, and in Equation 2.31 if $a > b$.

If the depth b of the trench in Figure 6(a) tends to infinity, the trench becomes a parallel-plate waveguide of semi-infinite length, and the field reflected at the bottom of the trench becomes a mode propagating in the positive $y-$direction inside the guide.

If the metal plane in Figure 6(c) is removed and only the metal strip exists, then the hori-

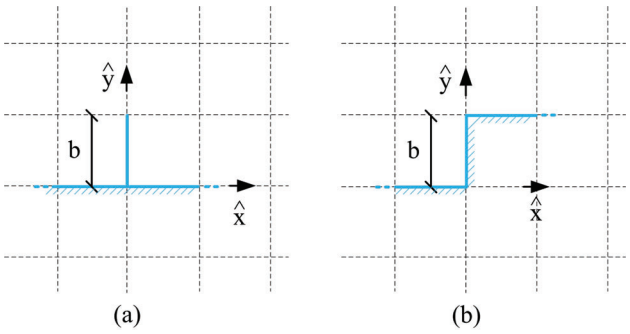

Figure 5. (a) Strip and (b) step on a metal plane.

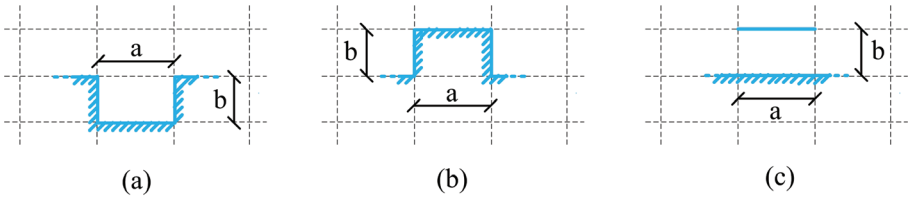

Figure 6. (a) Rectangular trench (b) rectangular ridge, and (c) strip on a metal plane.

zontal and vertical characteristic lengths are not exist any more and there is no need to apply conditions Equation 2.12 and Equation 2.11.

A peculiar structure is a finite or infinite array of equally spaced half-planes ($y \leq 0$) parallel to the $y-$axis with edges in the plane $y = 0$ as shown in Figure 7. The two incident waves 1 and 3 of Figure 1 and the condition Equation 2.11 assure the existence of the exact GO solutions. The two incident waves combine into a mode propagating in the negative $y-$direction between any two adjacent half-planes, and waves 2 and 4 of Figure 1 are not needed. The wavelength

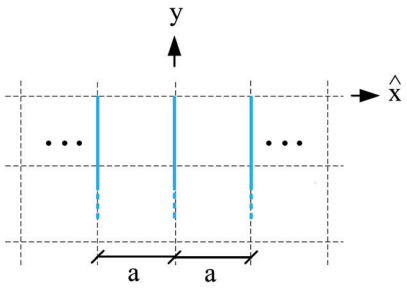

Figure 7. Finite of infinite array of half-planes.

condition $\lambda \leq 2a$ must be satisfied. There are m possible values for the incidence angle φ_0, which are given in Equation 2.30, where m is the integer that is used in Equation 2.11.

If the half-planes were thick instead of infinitesimally thin and truncated so as to have two right-angle wedges each, then a mode propagating in the positive $y-$direction would also have to be present, in order to have waves 2 and 4 incident on the right-angle wedges of the thick half-planes. This structure can be analyzed exactly under a single incident plane wave via the Wiener-Hopf method (see e.g. (10; 11; 36)); by combining two such solutions, the existence of an exact GO solution can be verified.

2.5 Three-Quadrant Structures

In all configurations where the metallic structure, with or without ridges and trenches, occupies the entire half-planes $(x \leq 0, y = 0)$ and $(x = 0, y \leq 0)$ without gaps, then the penetrable medium in contact with the structure occupies the first, second and fourth quadrants of space,

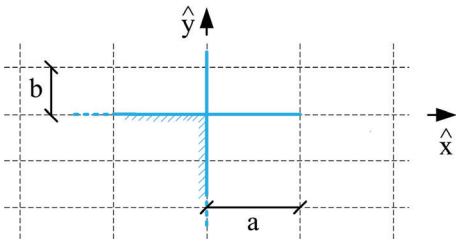

Figure 8. Right angle wedge with two metal baffles.

plus eventual trenches of finite depth. In these metallic structures, the three primary waves 1, 2 and 3 of Figure 1 are needed to assure the existence of an exact GO solution, the image wave 4 being reflection of waves 2 and 3 on the surfaces $(x = 0, y \leq 0)$ and $(x \leq 0, y = 0)$, respectively. The simplest three-quadrant structure is the right-angle wedge, previously discussed in (32). There are no characteristic lengths in the wedge structure, and hence no restrictions on ϕ_0 and λ are imposed.

If one or two metal baffles are present with the right-angle wedge as shown in Figure 8, then conditions Equation 2.11 and/or Equation 2.12 are required. For the metallic structure in Figure 8, both conditions are applied as characteristic lengths exist in the horizontal and vertical axis in this metallic structure. If $a \leq b$, then there are m possible values for the incidence angle φ_0, which are given in Equation 2.30. If $a > b$, then there are n possible values for the incidence angle and they are given in Equation 2.31.

A variety of more complicated three-quadrant structures may be created by inserting rectangular ridges and trenches, as well as metal strips, on the faces of a right-angle wedge. As an

example of such structure is the slotted wedge shown in Figure 9. For this structure, waves 1, 2 and 3 in Figure 1 are needed, while wave 4 being image of wave 2 and 3. Both conditions in Equation 2.11 and Equation 2.12 must be satisfied to get the exact GO solutions to the scattering problem. It is important to note that the parameters a, b and d must be commensurable to one another, the angle of incidence φ_0 is given by

$$\varphi_0 = \arctan\left(\frac{n\min(a,b,d)}{m\min(a,b,d)}\right) = \arctan\left(\frac{n}{m}\right) \tag{2.32}$$

where $\min(A,B)$ returns the minimum of A and B. The wavelength of the incident waves is given by

$$\lambda = \frac{2\min(a,b,d)}{\sqrt{m^2+n^2}} \tag{2.33}$$

and the wavelength condition in Equation 2.34 should be satisfied

$$\lambda \leq 2\min(a,b,d) \tag{2.34}$$

2.6 Four-Quadrant Structures

Aside from the half-plane, the simplest four-quadrant structures are the thick half-plane and the bent half-plane, shown in Figure 10. These structures only require condition Equation 2.11 to yield the exact GO solutions under incidence of all four waves in Figure 1. There are m possible values for the incidence angle φ_0, which are given in Equation 2.30. Also, they are

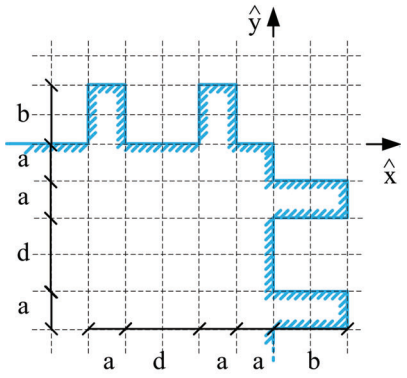

Figure 9. Slotted wedge.

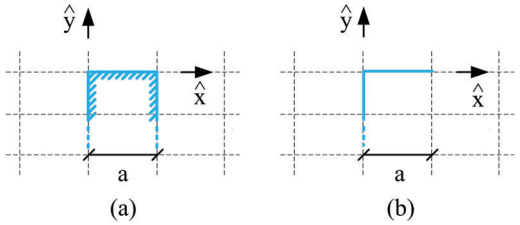

Figure 10. (a) Thick half-palne and (b) bent half-plane.

amenable to exact solution under a single incident plane wave, via the Wiener-Hopf function theoretic method (see e.g. (10; 11; 36)), meaning that repeated application of the Wiener-Hopf method to all four primary waves and summation of the four solutions leads to the GO solution. Simple structures requiring both condition Equation 2.11 and Equation 2.12 are the bent strip and the rectangular prism, shown in Figure 11. If $a \leq b$, there are m possible values for the incidence angle φ_0, which are given in Equation 2.30; while for $a > b$, there are n possible values

for the incidence angle φ_0 and they are given in Equation 2.31.

If the rectangular prism is surrounded by metallic planes from three sides as shown in Figure 12, the structure becomes parallel-plate waveguide. All the four primary waves of Figure 1 are needed to assure the existence of the exact GO solutions. The parameters a and d_1 must be commensurable to one another, as well as, parameters b, d_2 and d_3. Both conditions in Equation 2.11 and Equation 2.12 must be satisfied. There are two modes propagate in this structure, wave 1 and 2 combine and generate a mode propagates in the negative $x-$direction; while the reflections of wave 1 and 2 at the metal plane on the left side combine and generate a mode propagates in the positive $x-$direction. The angle of incidence φ_0 is given in Equation 2.35, the wavelength of the incident waves is give in Equation 2.36, which has a maximum possible value $\lambda \leq 2\min(a, b, d_1, d_2, d_3)$.

$$\tan\varphi_0 = \frac{n\min(a, d_1)}{m\min(b, d_2, d_3)} \tag{2.35}$$

$$\lambda = \frac{2}{\sqrt{\left(\frac{m}{\min(a, d_1)}\right)^2 + \left(\frac{n}{\min(b, d_2, d_3)}\right)^2}}. \tag{2.36}$$

Innumerable other four-quadrant structures, with simply or multiply connected cross-sectional shapes in any plane $z = constant$, can yield exact GO scattering solutions under excitation by four waves, provided that all linear dimensions in the same direction are commensurable to one another, i.e. the ratio of any two dimensions equals the ratio of two integer numbers. Examples of such structures are the L and I beams of Figure 13.

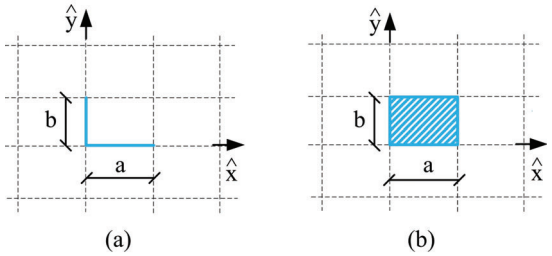

Figure 11. (a) Bent strip and (b) rectangular prism.

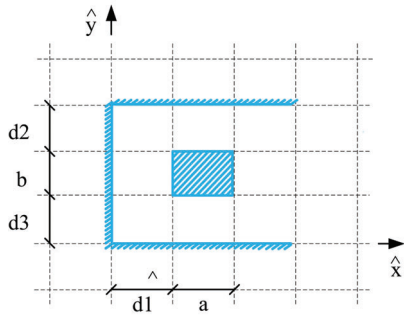

Figure 12. Prism surrounded by metallic planes from three sides.

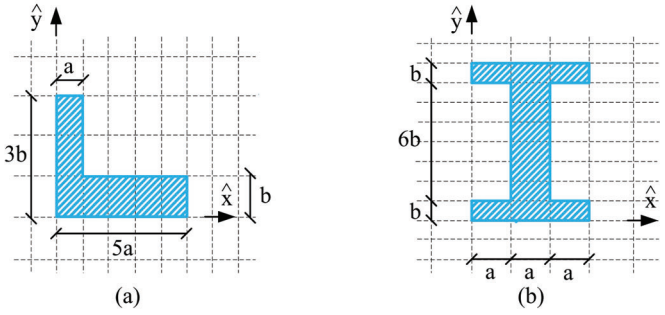

Figure 13. (a) L and (b) I beams.

2.7 General Steps to Apply Grid Method

The main steps to form the grid and apply the grid method to obtain the exact GO solutions to the scattering problem by metallic structures with strips and right-angle wedges under multiple plane waves excitation are summarized in the following:

- For the metallic structure under consideration, all the linear dimensions in the same direction (horizontal and vertical) need to be commensurable to one another.
- The grid is formed from identical rectangles with basic-lengths a and b along the horizontal ($x-$axis) and the vertical ($y-$axis) axis, respectively. It is recommended to set the basic-lengths a and b equal to the smallest characteristic length (smallest dimension) in the metallic structure along the horizontal and the vertical axis, respectively.
- All the widths of the metal strips in the $x-$direction must be multiples of the basic-length a, and all the widths of metal strips in the $y-$direction must be multiples of the basic-length b.
- After forming the grid, the metallic structure is placed on it, so that all the edges and strips in the metallic structure must be on the sides of the rectangles of the grid.
- If all the required conditions such as the number of the incident plane waves, the wavelength, the angle of incidence, the polarization of the incident waves, ...etc are satisfied, then the edges of the metallic structure under investigation do not scatter and the GO solution to the 2-D scattering problem is the exact solution.

- The obtained 2-D solution, which is obtained by grid method can be generalized to the 3-D solution by following the procedure detailed in (15).

CHAPTER 3

SCATTERING BY SPECIFIC METALLIC STRUCTURES WITH STRIPS AND RIGHT-ANGLE WEDGES EXCITED BY MULTIPLE INCIDENT PLANE WAVES

3.1 Introduction

The solution to the scattering problem by specific metallic structures consisting of strips and right-angle wedges are developed in this chapter based on the proposed grid method, which is presented in chapter 2. All the strips and edges in the metallic structures under investigation in this study extend indefinitely in the positive $z-$direction in the 3-D geometry; therefore, at any plane $z = constant$ and for all $z \geq 0$, the same 2-D geometry is obtained. All the metallic structures are assumed to be made of perfect electric conductor material, and are immersed in a lossless, homogeneous and isotropic medium such as free space.

To solve the scattering problem by these metallic structures, the 2-D solution is obtained based on the grid method first, then it is generalized to 3-D solution by considering an arbitrarily polarized plane wave, which is obliquely incident on the edges of the metallic structure, when the metallic structure is perpendicularly truncated by a ground plane. This is achieved by following the procedure in (15).

The incident plane waves propagate in a linear, homogeneous and isotropic medium. Two types of polarization are considered. E-polarization, when the $z-$component of the magnetic

field is zero (electric field everywhere is parallel to the edges of the metallic structure), and H-polarization, when the $z-$component of the electric field is zero (magnetic field everywhere is parallel to the edges of the metallic structure). The primary incident plane wave 1 of Figure 1 propagates in the direction $\hat{k}^{i1}$, which forms the angle θ_0 with the negative $z-$axis; while the projection of $\hat{k}^{i1}$ onto the plane $z = 0$ forms the angle φ_0 with the negative $x-$axis. The direction of propagation of the four incident plane waves are $\hat{k}^{i1}$, $\hat{k}^{i2}$, $\hat{k}^{i3}$ and $\hat{k}^{i4}$, which are given by

$$\hat{k}^{i1} = -\hat{x}\sin\theta_0\cos\varphi_0 - \hat{y}\sin\theta_0\sin\varphi_0 - \hat{z}\cos\theta_0 \tag{3.1}$$

$$\hat{k}^{i2} = -\hat{x}\sin\theta_0\cos\varphi_0 + \hat{y}\sin\theta_0\sin\varphi_0 - \hat{z}\cos\theta_0 \tag{3.2}$$

$$\hat{k}^{i3} = \hat{x}\sin\theta_0\cos\varphi_0 - \hat{y}\sin\theta_0\sin\varphi_0 - \hat{z}\cos\theta_0 \tag{3.3}$$

$$\hat{k}^{i4} = \hat{x}\sin\theta_0\cos\varphi_0 + \hat{y}\sin\theta_0\sin\varphi_0 - \hat{z}\cos\theta_0. \tag{3.4}$$

The key point to select the electric field of the four incident plane waves in the grid method for the E-polarization is that: for the four incident plane waves shown in Figure 1, plane waves 2 and 3 are 180^o out-of-phase with respect to plane wave 1; while plane wave 4 is in-phase

with the plane wave 1 at all edges of the metallic structure. Thus, the electric field of the four incident plane waves for the E-polarization is assigned as

$$\underline{\mathbf{E}}^{(\mathbf{e})\mathbf{i1}} = (-\hat{x}\cos\theta_0\cos\varphi_0 - \hat{y}\cos\theta_0\sin\varphi_0 + \hat{z}\sin\theta_0)e^{-jk\hat{k}^{i1}\cdot\underline{r}} \tag{3.5}$$

$$\underline{\mathbf{E}}^{(\mathbf{e})\mathbf{i2}} = (\hat{x}\cos\theta_0\cos\varphi_0 - \hat{y}\cos\theta_0\sin\varphi_0 - \hat{z}\sin\theta_0)e^{-jk\hat{k}^{i2}\cdot\underline{r}} \tag{3.6}$$

$$\underline{\mathbf{E}}^{(\mathbf{e})\mathbf{i3}} = (-\hat{x}\cos\theta_0\cos\varphi_0 + \hat{y}\cos\theta_0\sin\varphi_0 - \hat{z}\sin\theta_0)e^{-jk\hat{k}^{i3}\cdot\underline{r}} \tag{3.7}$$

$$\underline{\mathbf{E}}^{(\mathbf{e})\mathbf{i4}} = (\hat{x}\cos\theta_0\cos\varphi_0 + \hat{y}\cos\theta_0\sin\varphi_0 + \hat{z}\sin\theta_0)e^{-jk\hat{k}^{i4}\cdot\underline{r}} \tag{3.8}$$

the corresponding magnetic field can be found by Maxwell's equations. The magnitude of the electric field of incident waves is assumed to be 1 V/m.

For the H-polarization, the key point to choose the magnetic field of the four incident plane waves in the grid method is that: the magnetic field of all the four plane waves of Figure 1 should be in-phase at all edges of the metallic structure. Thus, the magnetic field of the four incident plane waves for the H-polarization is chosen to be

$$\underline{\mathbf{H}}^{(\mathbf{h})\mathbf{i1}} = Y(-\hat{x}\cos\theta_0\cos\varphi_0 - \hat{y}\cos\theta_0\sin\varphi_0 + \hat{z}\sin\theta_0)e^{-jk\hat{k}^{i1}\cdot\underline{r}} \tag{3.9}$$

$$\underline{\mathbf{H}}^{(\mathbf{h})\mathbf{i2}} = Y(-\hat{x}\cos\theta_0\cos\varphi_0 + \hat{y}\cos\theta_0\sin\varphi_0 + \hat{z}\sin\theta_0)e^{-jk\hat{k}^{i2}\cdot\underline{r}} \tag{3.10}$$

$$\underline{\mathbf{H}}^{(\mathbf{h})\mathbf{i3}} = Y(\hat{x}\cos\theta_0\cos\varphi_0 - \hat{y}\cos\theta_0\sin\varphi_0 + \hat{z}\sin\theta_0)e^{-jk\hat{k}^{i3}\cdot\underline{r}} \tag{3.11}$$

$$\underline{\mathbf{H}}^{(\mathbf{h})\mathbf{i4}} = Y(\hat{x}\cos\theta_0\cos\varphi_0 + \hat{y}\cos\theta_0\sin\varphi_0 + \hat{z}\sin\theta_0)e^{-jk\hat{k}^{i4}\cdot\underline{r}} \tag{3.12}$$

$$Z = \frac{1}{Y} = \sqrt{\frac{\mu}{\epsilon}} \tag{3.13}$$

$$\underline{r} = x\hat{x} + y\hat{y} + z\hat{z} \tag{3.14}$$

where Z and Y are the intrinsic impedance and admittance of the medium, respectively.

In the two-dimensional geometry, the incidence is normal to the edges of the metallic structure ($\theta_0 = \pi/2$). The electric field of the four incident plane waves in 2-D geometry is given in Equation 2.1 to Equation 2.4 for the E-polarization, and the magnetic field is given in Equation 2.14 to Equation 2.17 for the H-polarization.

If the 2-D solution to the boundary-value problem, which is obtained by applying the grid method is given by $U^{(e)} = (x, y; k)$ and $U^{(h)} = (x, y; k)$ for the E-polarization and the H-polarization, respectively, then by following the procedure in (15), it is possible to obtain the 3-D solution to the scattering problem when an arbitrarily polarized plane wave is obliquely incident upon the edges of the metallic structure when the latter is truncated perpendicularly by a ground plane at $z = 0$. The direction of propagation of the primary incident wave 1 forms the angle θ_0 with the negative $z-$axis; while its projection onto the xy plane forms the angle

φ_0 with the negative $x-$axis. Based on the general procedure in (15), the 3-D solution can be obtained as shown in Equation 3.15 and Equation 3.16 for E-polarization

$$\underline{\mathbf{E}}^{(\mathbf{e})} = \left[-\frac{2}{k}\cot\theta_0 \sin\left(kz\cos\theta_0\right)\left(\hat{x}\frac{\partial}{\partial x}+\hat{y}\frac{\partial}{\partial y}\right)+2\sin\theta_0\cos\left(kz\cos\theta_0\right)\hat{z}\right]\times$$
$$U^{(e)}(x,y;k\sin\theta_0) \tag{3.15}$$

$$\underline{\mathbf{H}}^{(\mathbf{e})} = \frac{2jY}{k\sin\theta_0}\cos\left(kz\cos\theta_0\right)\left(\hat{x}\frac{\partial}{\partial y}-\hat{y}\frac{\partial}{\partial x}\right)\times U^{(e)}(x,y;k\sin\theta_0) \tag{3.16}$$

and for the H-polarization is given in Equation 3.17 and Equation 3.18 (15)

$$\underline{\mathbf{E}}^{(\mathbf{h})} = \frac{2}{k\sin\theta_0}\sin\left(kz\cos\theta_0\right)\left(\hat{x}\frac{\partial}{\partial y}-\hat{y}\frac{\partial}{\partial x}\right)\times U^{(h)}(x,y;k\sin\theta_0) \tag{3.17}$$

$$\underline{\mathbf{H}}^{(\mathbf{h})} = \left[\frac{2jY}{k}\cot\theta_0\cos\left(kz\cos\theta_0\right)\left(\hat{x}\frac{\partial}{\partial x}+\hat{y}\frac{\partial}{\partial y}\right)+2jY\sin\theta_0\sin\left(kz\cos\theta_0\right)\hat{z}\right]\times$$
$$U^{(h)}(x,y;k\sin\theta_0). \tag{3.18}$$

3.2 Two Parallel Semi-infinite Metal Plates

Assume two parallel semi-infinite metal plates extending in the negative $y-$direction with separation distance a between them. To construct the grid, all the characteristic lengths in the metallic structure need to be defined. In this structure, there is only one characteristic length, which is the separation distance a in the direction of the $x-$axis. Thus, there is no limitation regarding the vertical basic-length (in the $y-$axis) of the grid; while the horizontal basic-length (in the $x-$axis) of the grid's elements (rectangles) should be equal to the separation distance a as one of the required conditions to assure that the obtained GO solutions are the exact

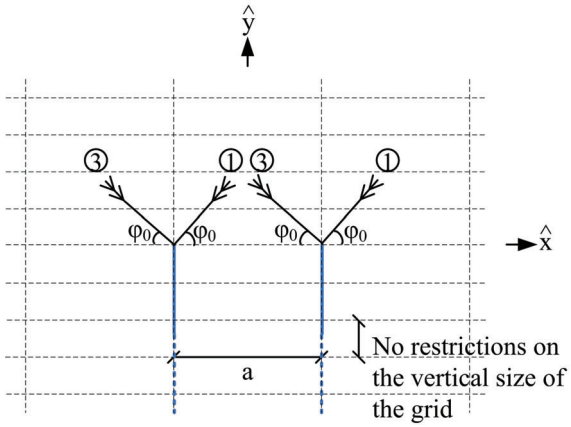

Figure 14. Pair of parallel semi-infinite metal plates with the gride structure.

solutions to the scattering problem. It is possible to choose the horizontal basic-length to be less than a, but the ratio of the horizontal characteristic length of the metallic structure to the horizontal basic-length of the grid's elements must be an integer number. It is recommended to choose the horizontal basic-length of the grid's elements to be equal to a in order to lower the minimum value of frequency for which GO solution is possible. The 2-D geometry with the grid sketched in broken lines is shown in Figure 14. Since there is only one characteristic length in the horizontal axis in this structure, which is the separation distance a, only condition Equation 2.11 applies and only wave 1 and 3 of Figure 1 are needed. Based on the value of the integer m in Equation 2.11, there will be m possible values for the angle of incidence φ_0, which are obtained by Equation 2.30. The wavelength of the incident waves should satisfy the wavelength condition $\lambda \leq 2a$.

3.2.1 Solution to the E-polarization

If all the conditions in the previous section are satisfied, then and based on the grid method, the total 2-D electric field is given in Equation 3.19. It is the sum of the electric field of the two incident plane waves, which are given in Equation 2.1 and Equation 2.3. The corresponding total 2-D magnetic field follows from Maxwell's equations. The total 2-D field has one TE mode, which travels in the negative $y-$direction between the two parallel semi-infinite plates.

$$\begin{aligned}\underline{E}^{(e)t}|_{2-D} = E_z^{(e)i1} + E_z^{(e)i2} =& e^{jk(x\cos\varphi_0 + y\sin\varphi_0)}\hat{z} - e^{-jk(x\cos\varphi_0 - y\sin\varphi_0)}\hat{z} \\ =& \hat{z}\ 2j\ e^{jky\sin\varphi_0}\sin(kx\cos\varphi_0) \end{aligned} \tag{3.19}$$

The 2-D solution $U^{(e)}(x, y; k)$ in Equation 3.19 is generalized to the 3-D solution when the metallic structure is perpendicularly truncated by a metal ground plate by following the producer in (15). The 3-D geometry of the metallic structure is shown in Figure 15. By using Equation 3.15, Equation 3.16, and Equation 3.19, the total 3-D electric $\underline{\mathbf{E}}^{(\mathbf{e})}$ and magnetic $\underline{\mathbf{H}}^{(\mathbf{e})}$ fields are found to be

$$\begin{aligned}\underline{\mathbf{E}}^{(\mathbf{e})} =& -4\cos\theta_0\sin(kz\cos\theta_0)\sin(kx\sin\theta_0\cos\varphi_0)\, e^{jky\sin\theta_0\sin\varphi_0} \\ & [\hat{x}j\cos\varphi_0\cot(kx\sin\theta_0\cos\varphi_0) - \hat{y}\sin\varphi_0 + \hat{z}j\tan\theta_0\cot(kz\cos\theta_0)] \end{aligned} \tag{3.20}$$

$$\begin{aligned}\underline{\mathbf{H}}^{(\mathbf{e})} =& -4jY\cos(kz\cos\theta_0)\, e^{jky\sin\theta_0\sin\varphi_0} \\ & [\hat{x}\sin\varphi_0\sin(kx\sin\theta_0\cos\varphi_0) + \hat{y}j\cos\varphi_0\cos(kx\sin\theta_0\cos\varphi_0)]\,. \end{aligned} \tag{3.21}$$

The surface current density on the truncating plate can be obtained from $\underline{\mathbf{J}}^{(\mathbf{e})} = \hat{n} \times \underline{\mathbf{H}}^{(\mathbf{e})}$, where $\hat{n} = \hat{z}$ is the unit normal pointing away from the metallic surface, thus

$$\underline{\mathbf{J}}^{(\mathbf{e})}|_{z=0} = \hat{z} \times \underline{\mathbf{H}}^{(\mathbf{e})} = -4jYe^{jky\sin\theta_0\sin\varphi_0} \\ [-\hat{x}j\cos\varphi_0\cos(kx\sin\theta_0\cos\varphi_0) + \hat{y}\sin\varphi_0\sin(kx\sin\theta_0\cos\varphi_0)] \quad (3.22)$$

Figure 16 shows the magnitude of the $x-$component of the surface current density $\underline{\mathbf{J}}^{(\mathbf{e})}$ on the truncating plate $z = 0$ between the two parallel plates for the E-polarization case when the separation distance $a = \lambda$ and the angles of incidence are $\theta_0 = \pi/6$ and $\varphi_0 = \pi/3$. It can be seen that, $J_x^{(e)}$ has maximum value along the intersection of the parallel plates with the truncating plate at $x = \pm a/2$, $-10\lambda \leq y \leq 0$ and $z = 0$, as at the intersection, $J_x^{(e)}$ moves towards the parallel plates to avoid charge accumulation at the edges and to assure the continuity of the current density across the edges of the metal structure. The currents that are perpendicular to the edges of the metallic structure are continuous across the edges, which is the case of $J_x^{(e)}$. Figure 17 shows the $y-$component of the surface current density $\underline{\mathbf{J}}^{(\mathbf{e})}$ between the two parallel plates on the truncating plate $z = 0$. It can be shown that the $y-$component of surface current density, which is parallel to the edges of the metallic structure vanishes along the intersection of the parallel plates with the truncating plate at $x = \pm a/2$, $-10\lambda \leq y \leq 0$ and $z = 0$.

The problem of the scattering of a single electromagnetic plane wave incident on the edges of two parallel semi-infinite metal plates was solved using the Wiener-Hopf theoretic method in 2-D geometry in (10; 11), and in 3-D geometry in (14). It can be proven that the grid method

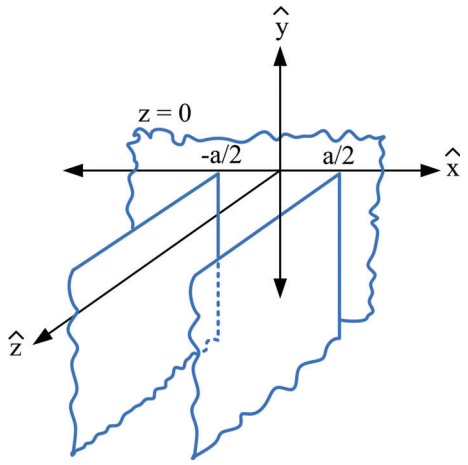

Figure 15. Three-dimensional geometry of the metallic structure.

develops the exact GO solutions to the boundary-value problem under multiple incident plane waves by solving the problem analytically using the Wiener-Hopf theoretic method for each incident plane wave individually, then adding the individual solutions to get the total solution to the problem as shown below.

When the incident plane wave is given by Equation 2.1, by using Wiener-Hopf method (10; 11), the 2-D solution is found to be

$$\underline{E}^{(e)t1}|_{2-D} = e^{jk(x\cos\varphi_0 + y\sin\varphi_0)} - \frac{1}{\sqrt{2\pi}}\int \left[S1_{-}\cosh(\gamma x) + D1_{-}\sinh(\gamma x)\right] e^{-\gamma\frac{a}{2}} e^{-j\alpha y}, \qquad -a/2 \le x \le a/2 \tag{3.23}$$

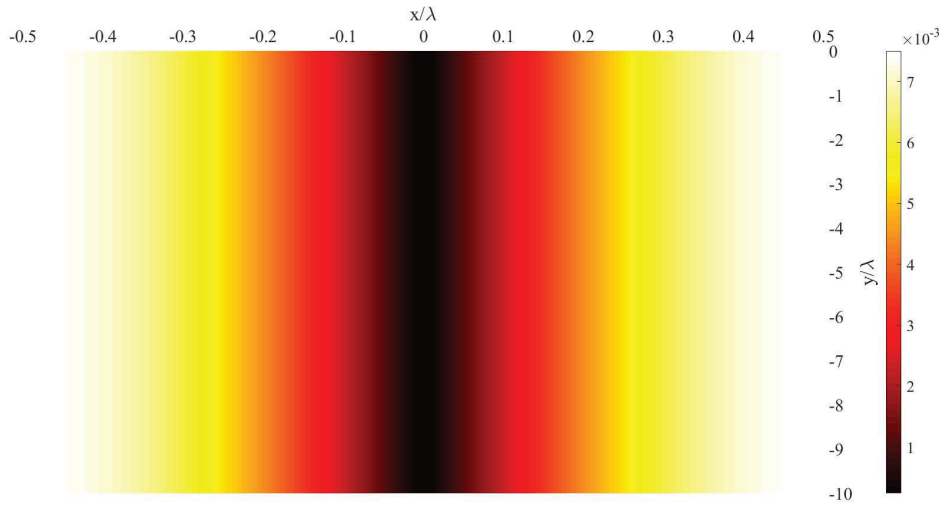

Figure 16. Magnitude of $J_x^{(e)}$ on the truncating plate $z = 0$ between the pair of semi-infinite plates for E-polarization when $a = \lambda$, $\theta_0 = \pi/6$ and $\varphi_0 = \pi/3$.

$$\underline{E}^{(e)t1}|_{2-D} = e^{jk(x\cos\varphi_0 + y\sin\varphi_0)} - \frac{1}{\sqrt{2\pi}} \int \left[S1_- \sinh(\gamma\frac{a}{2}) - D1_- \cosh(\gamma\frac{a}{2}) \right] e^{-\gamma x} e^{-j\alpha y}, \qquad -\infty \le x \le -a/2 \tag{3.24}$$

$$\underline{E}^{(e)t1}|_{2-D} = e^{jk(x\cos\varphi_0 + y\sin\varphi_0)} - \frac{1}{\sqrt{2\pi}} \int \left[S1_- \sinh(\gamma\frac{a}{2}) + D1_- \cosh(\gamma\frac{a}{2}) \right] e^{-\gamma x} e^{-j\alpha y}, \qquad +a/2 \le x \le +\infty \tag{3.25}$$

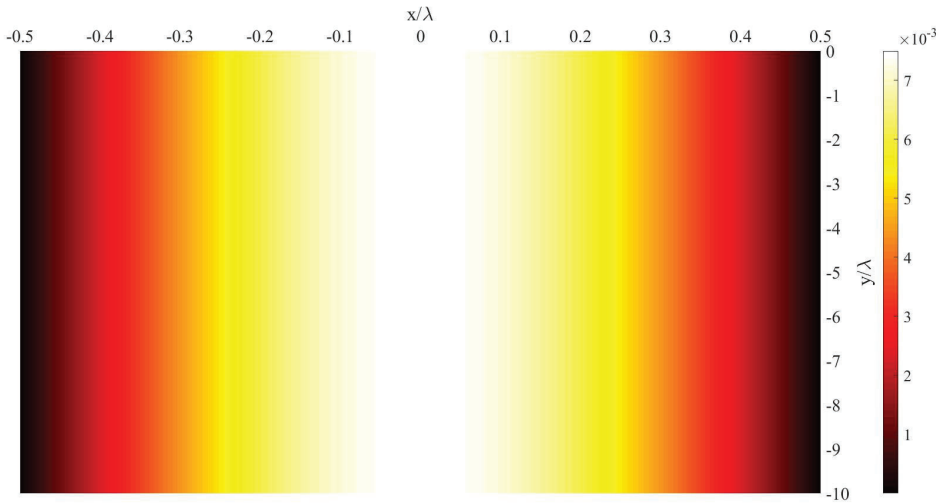

Figure 17. Magnitude of $J_y^{(e)}$ on the truncating plate $z = 0$ between the pair of semi-infinite plates for E-polarization when $a = \lambda$, $\theta_0 = \pi/6$ and $\varphi_0 = \pi/3$.

For the second incident plane wave Equation 2.3, the 2-D solution is found to be

$$\underline{E}^{(e)t2}|_{2-D} = -\, e^{-jk(x\cos\varphi_0 - y\sin\varphi_0)} - \frac{1}{\sqrt{2\pi}} \int \left[S2_- \cosh(\gamma x) + D2_- \sinh(\gamma x)\right] e^{-\gamma\frac{a}{2}} e^{-j\alpha y}, \qquad -a/2 \le x \le a/2 \tag{3.26}$$

$$\underline{E}^{(e)t2}|_{2_D} = - e^{-jk(x\cos\varphi_0 - y\sin\varphi_0)} - \frac{1}{\sqrt{2\pi}} \int \left[S2_- \sinh(\gamma\frac{a}{2}) - D2_- \cosh(\gamma\frac{a}{2}) \right] e^{-\gamma x} e^{-j\alpha y}, \qquad -\infty \le x \le -a/2 \tag{3.27}$$

$$\underline{E}^{(e)t2}|_{2_D} = - e^{-jk(x\cos\varphi_0 - y\sin\varphi_0)} - \frac{1}{\sqrt{2\pi}} \int \left[S2_- \sinh(\gamma\frac{a}{2}) + D2_- \cosh(\gamma\frac{a}{2}) \right] e^{-\gamma x} e^{-j\alpha y}, \qquad +a/2 \le x \le +\infty \tag{3.28}$$

$S1_-$, $S2_-$, $D1_-$ and $D2_-$ are found to be

$$S1_- = -S2_- = \frac{ik\sin\varphi_0 \sin\left(k\frac{a}{2}\sin\varphi_0\right)}{\sqrt{2\pi}\sqrt{(k+k\cos\varphi_0)}\ K_+(k\cos\varphi_0)\sqrt{\alpha-k}\ K_-(\alpha)\ (\alpha - k\cos\varphi_0)} \tag{3.29}$$

$$D1_- = -D2_- = \frac{k\sin\varphi_0 \cos\left(k\frac{a}{2}\sin\varphi_0\right)}{\sqrt{2\pi}\sqrt{(k+k\cos\varphi_0)}\ L_+(k\cos\varphi_0)(\alpha-k)\ L_-(\alpha)\ (\alpha - k\cos\varphi_0)} \tag{3.30}$$

adding the two sub-solutions of the same region, yields the total 2-D solution

$$\underline{E}^{(e)t}|_{2_D} = \underline{E}^{(e)t1}|_{2-D} + \underline{E}^{(e)t2}|_{2_D} = \hat{z}\ e^{jk(x\cos\varphi_0 + y\sin\varphi_0)} - \hat{z}\ e^{-jk(x\cos\varphi_0 - y\sin\varphi_0)}, \tag{3.31}$$

which is the same result in Equation 3.19, that was obtained by applying the grid method. This verifies that the obtained geometrical optics solution using the grid method is indeed the exact

solution to the boundary-value problem.

3.2.2 Solution to the H-polarization

For the H-polarization and based on the grid method, the total magnetic field is the sum of the magnetic field of the two incident plane waves, which are given in Equation 2.14 and Equation 2.16. The related total 2-D electric field follows from Maxwell's equations. The total 2-D magnetic field is given in Equation 3.32, which has one TM mode propagates in the negative $y-$direction.

$$\begin{aligned}\underline{H}^{(h)t}|_{2-D} = H_z^{(h)i1} + H_z^{(h)i2} =& Y e^{jk(x\cos\varphi_0 + y\sin\varphi_0)}\,\hat{z} + Y e^{-jk(x\cos\varphi_0 - y\sin\varphi_0)}\,\hat{z} \\ =& \hat{z}\; 2Y e^{jky\sin\varphi_0}\cos\left(kx\cos\varphi_0\right). \end{aligned} \tag{3.32}$$

The total 2-D solution $U^{(h)}(x,y;k) = ZH_{2-D}^{(h)t}$ in Equation 3.32 is generalized to the 3-D solution by using the same procedure that is used for the E-polarization, yields the total 3-D electric $\underline{\mathbf{E}}^{(\mathbf{h})}$ and magnetic $\underline{\mathbf{H}}^{(\mathbf{h})}$ fields

$$\begin{aligned}\underline{\mathbf{E}}^{(\mathbf{h})} =& 4\sin\left(kz\cos\theta_0\right) e^{jky\sin\theta_0\sin\varphi_0} \\ & \left[\hat{x}j\sin\varphi_0\cos\left(kx\sin\theta_0\cos\varphi_0\right) + \hat{y}\cos\varphi_0\sin\left(kx\sin\theta_0\cos\varphi_0\right)\right] \end{aligned} \tag{3.33}$$

$$\begin{aligned}\underline{\mathbf{H}}^{(\mathbf{h})} =& 4Y\cos\theta_0\cos\left(kz\cos\theta_0\right)\cos\left(kx\sin\theta_0\cos\varphi_0\right) e^{jky\sin\theta_0\sin\varphi_0} \\ & \left[-\hat{x}\cos\varphi_0\tan\left(kx\sin\theta_0\cos\varphi_0\right) + \hat{y}j\sin\varphi_0 + \hat{z}j\tan\theta_0\tan\left(kz\cos\theta_0\right)\right]. \end{aligned} \tag{3.34}$$

The surface current density on the truncating plate can be obtained from $\underline{\mathbf{J}}^{(\mathbf{h})} = \hat{z} \times \underline{\mathbf{H}}^{(\mathbf{h})}$, thus

$$\underline{\mathbf{J}}^{(\mathbf{h})}|_{z=0} = -4Y \cos\theta_0 e^{jky \sin\theta_0 \sin\varphi_0} \\ [\hat{x} j \sin\varphi_0 \cos(kx \sin\theta_0 \cos\varphi_0) + \hat{y} \cos\varphi_0 \sin(kx \sin\theta_0 \cos\varphi_0)] \tag{3.35}$$

Figure 18 and Figure 19 show the magnitude of the x- and y-component of the surface current density $\underline{\mathbf{J}}^{(\mathbf{h})}$ on the truncating plate $z = 0$ between the two parallel plates for the case of H-polarization when the separation distance $a = \lambda$ and the angles of incidence are $\theta_0 = \pi/6$ and $\varphi_0 = \pi/3$, respectively.

For the H-polarization, a similar analytical result can be obtained by using the same analytical method (the Wiener-Hopf theoretic method) that is used for the E-polarization. When the incident plane wave is given by Equation 2.14, the 2-D solution is found to be

$$\underline{H}^{(h)t1}|_{2-D} = e^{jk(x\cos\varphi_0 + y\sin\varphi_0)} \\ - \frac{1}{\sqrt{2\pi}} \int [S1_- \cosh(\gamma x) + D1_- \sinh(\gamma x)]\, e^{-\gamma \frac{a}{2}} e^{-j\alpha y}, \qquad -a/2 \le x \le a/2 \tag{3.36}$$

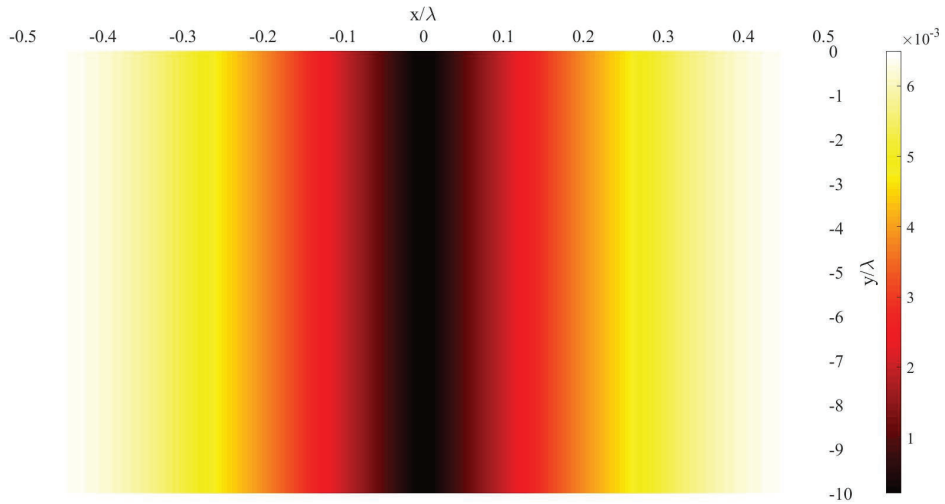

Figure 18. Magnitude of $J_x^{(h)}$ on the truncating plate $z = 0$ between the pair of semi-infinite plates for H-polarization when $a = \lambda$, $\theta_0 = \pi/6$ and $\varphi_0 = \pi/3$.

$$\underline{H}^{(h)t1}|_{2-D} = e^{jk(x\cos\varphi_0 + y\sin\varphi_0)} - \frac{1}{\sqrt{2\pi}} \int \left[S1_- \sinh(\gamma\frac{a}{2}) - D1_- \cosh(\gamma\frac{a}{2}) \right] e^{-\gamma x} e^{-j\alpha y}, \qquad -\infty \le x \le -a/2 \tag{3.37}$$

$$\underline{H}^{(h)t1}|_{2-D} = e^{jk(x\cos\varphi_0 + y\sin\varphi_0)} - \frac{1}{\sqrt{2\pi}} \int \left[S1_- \sinh(\gamma\frac{a}{2}) + D1_- \cosh(\gamma\frac{a}{2}) \right] e^{-\gamma x} e^{-j\alpha y}, \qquad +a/2 \le x \le +\infty \tag{3.38}$$

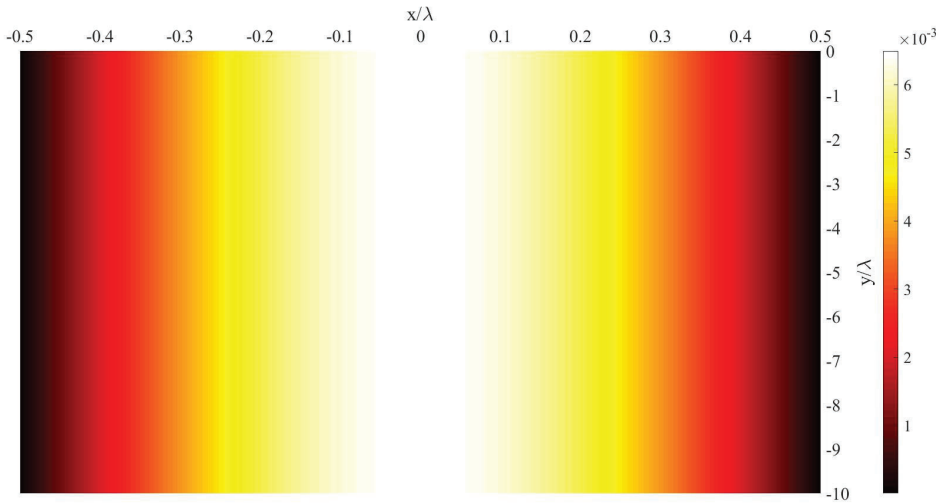

Figure 19. Magnitude of $J_y^{(h)}$ on the truncating plate $z = 0$ between the pair of semi-infinite plates for H-polarization when $a = \lambda$, $\theta_0 = \pi/6$ and $\varphi_0 = \pi/3$.

For the second incident plane wave Equation 2.16, the 2-D solution is found to be

$$\underline{H}^{(h)t2}|_{2-D} = e^{-jk(x\cos\varphi_0 - y\sin\varphi_0)} - \frac{1}{\sqrt{2\pi}} \int \left[S2_- \cosh(\gamma x) + D2_- \sinh(\gamma x)\right] e^{-\gamma\frac{a}{2}} e^{-j\alpha y}, \qquad -a/2 \le x \le a/2 \tag{3.39}$$

$$\underline{H}^{(h)t2}|_{2-D} = e^{-jk(x\cos\varphi_0 - y\sin\varphi_0)} - \frac{1}{\sqrt{2\pi}}\int \left[S2_- \sinh(\gamma\frac{a}{2}) - D2_- \cosh(\gamma\frac{a}{2})\right] e^{-\gamma x} e^{-j\alpha y}, \qquad -\infty \le x \le -a/2 \tag{3.40}$$

$$\underline{H}^{(h)t2}|_{2-D} = e^{-jk(x\cos\varphi_0 - y\sin\varphi_0)} - \frac{1}{\sqrt{2\pi}}\int \left[S2_- \sinh(\gamma\frac{a}{2}) + D2_- \cosh(\gamma\frac{a}{2})\right] e^{-\gamma x} e^{-j\alpha y}, \qquad +a/2 \le x \le +\infty \tag{3.41}$$

adding the two sub-solutions of the same region and multiply it by Y, yields the total 2-D solution

$$Y\underline{H}^{(h)t}|_{2-D} = Y\underline{H}^{(h)t1}|_{2-D} + Y\underline{H}^{(h)t2}|_{2-D} = \hat{z}\ Ye^{jk(x\cos\varphi_0 + y\sin\varphi_0)} + \hat{z}\ Ye^{-jk(x\cos\varphi_0 - y\sin\varphi_0)}, \tag{3.42}$$

which is the same result in Equation 3.32, that was obtained by applying the grid method.

3.3 Finite (or Infinite) Array of Equally Spaced Semi-infinite Metal Plates

For an array consisting of finite (or infinite) number of semi-infinite metal plates, which are equally spaced with a separation distance between any two adjacent plates a, only wave 1 and wave 3 of Figure 1 are required and the other waves 2 and 4 are not needed to obtain the exact GO solutions. There is only one characteristic length in this structure, which is the

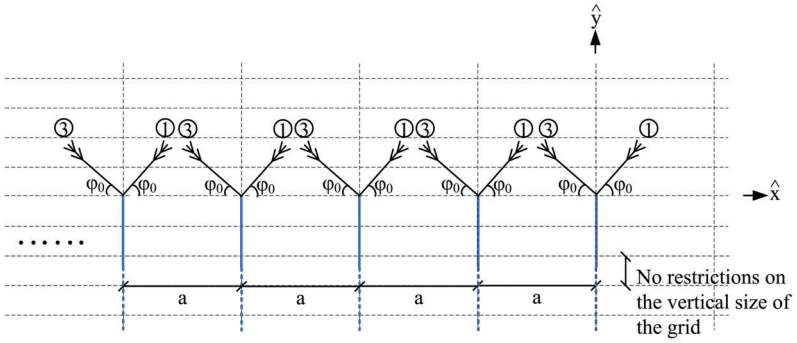

Figure 20. Two-dimensional geometry of an array of $N = 4$ equally spaced semi-infinite parallel metal plates with the grid structure.

separation distance a between any two adjacent plates in the $x-$axis (the horizontal axis); while there is no characteristic length along the $y-$axis (the vertical axis). To construct the grid, the best choice for the horizontal basic-length of the rectangles (grid's elements) is to be equal to the smallest characteristic length along the horizontal axis, which is the separation distance a. On the other side, since there is no characteristic length along the vertical axis, there is no restriction about the vertical basic-length and it can take any value. Figure 20 shows the two-dimensional geometry of the structure with the appropriate grid structure. Only condition Equation 2.11 applies as there is only one characteristic length along the horizontal axis in the metallic structure. The wavelength of the incident waves should satisfy the wavelength condition $\lambda \leq 2a$. There are m possible values for the angle of incidence φ_0, which can be computed by using Equation 2.30, where m is the integer that is used in Equation 2.11.

3.3.1 Solution to the E-polarization

If all the conditions related to the wavelength, angle of incidence, polarization, ... etc are satisfied and the grid is constructed correctly, then by the grid method, the total 2-D electric field is given in Equation 3.19. It is the sum of the electric fields of the two incident plane waves, which are given in Equation 2.1 and Equation 2.3. The incident waves combine to generate a TE mode, that propagates in the negative $y-$direction between any two adjacent parallel plates. The corresponding total 2-D magnetic field can be found from Maxwell's equations.

In general, for an array of N (N is finite or infinite) equally spaced semi-infinite metal plates with separation distance between each two adjacent plates a, the total 2-D and 3-D fields in the region between the semi-infinite metal plates $-a(N-1) \leq x \leq 0$, $-\infty \leq y \leq +\infty$ and $0 \leq z \leq +\infty$ can be found by using the semi-periodicity relation in (13); which yields the following total 2-D fields:

$$E_z^{(e)t}(x,y;k) = \sum_{q=0}^{q=N-2} e^{-jkqa\sin\varphi_0} E_z^{(e)1}(x-qa,y;k) \tag{3.43}$$

$$H_z^{(e)t}(x,y;k) = \sum_{q=0}^{q=N-2} e^{-jkqa\sin\varphi_0} H_z^{(e)1}(x-qa,y;k) \tag{3.44}$$

where $E_z^{(e)1}(x,y;k)$ is the 2-D electric field between the first two plates $-a \leq x \leq 0$, $-\infty \leq y \leq +\infty$ and $0 \leq z \leq +\infty$, which is the sum of the electric field of the two incident waves given in Equation 2.1 and Equation 2.3 based on the grid method. The corresponding 2-D magnetic field $H_z^{(e)1}(x,y;k)$ follows from Maxwell's equations.

The 2-D solution is extended to 3-D solution based on the procedure in (15), which yields the following total 3-D fields:

$$\underline{\mathbf{E}}^{(\mathbf{e})\mathbf{t}}(x,y,z) = \sum_{q=0}^{q=N-2} e^{-jkqa\sin\varphi_0\sin\theta_0}\underline{\mathbf{E}}^{(\mathbf{e})\mathbf{1}}(x-qa,y,z) \tag{3.45}$$

$$\underline{\mathbf{H}}^{(\mathbf{e})\mathbf{t}}(x,y,z) = \sum_{q=0}^{q=N-2} e^{-jkqa\sin\varphi_0\sin\theta_0}\underline{\mathbf{H}}^{(\mathbf{e})\mathbf{1}}(x-qa,y,z) \tag{3.46}$$

where $\underline{\mathbf{E}}^{(\mathbf{e})\mathbf{1}}(x,y,z)$ and $\underline{\mathbf{H}}^{(\mathbf{e})\mathbf{1}}(x,y,z)$ are the 3-D electric and the 3-D magnetic field between the first two plates $0 \leq x \leq -a$, $-\infty \leq y \leq +\infty$ and $0 \leq z \leq +\infty$, which are found by following the general procedure in (15), and using the 2-D solution that is obtained by the grid method.

3.3.2 Solution to the H-polarization

The same analysis that is used for the E-polarization can be used for the H-polarization. All the conditions that are applied to the E-polarization case, are applied to the H-polarization too. Based on the grid method, the total 2-D magnetic field is the sum of the magnetic fields of the two incident plane waves, which are given in Equation 2.14 and Equation 2.16. The two waves combine to generate a TM mode that propagates in the negative $y-$direction between any two adjacent semi-infinite parallel plates. The corresponding total 2-D electric field follows from Maxwell's equations.

The total 2-D and 3-D fields in the region between the semi-infinite metal plates

$0 \leq x \leq -a(N-1)$, $-\infty \leq y \leq +\infty$ and $0 \leq z \leq +\infty$ can be found by using the semi-periodicity relation in (13), which yields the following 2-D fields:

$$E_z^{(h)t}(x,y;k) = \sum_{q=0}^{q=N-2} e^{-jkqa\sin\varphi_0} E_z^{(h)1}(x-qa,y;k) \tag{3.47}$$

$$H_z^{(h)t}(x,y;k) = \sum_{q=0}^{q=N-2} e^{-jkqa\sin\varphi_0} H_z^{(h)1}(x-qa,y;k) \tag{3.48}$$

where $H_z^{(h)1}(x,y;k)$ is the 2-D magnetic field between the first two plates $0 \leq x \leq -a$, $-\infty \leq y \leq +\infty$ and $0 \leq z \leq +\infty$, which is the sum of the magnetic field of the two incident waves, which are given in Equation 2.14 and Equation 2.16 based on the grid method. The related 2-D electric field $E_z^{(h)1}(x,y;k)$ can be found from Maxwell's equations. The total 3-D fields are given by

$$\underline{\mathbf{E}}^{(\mathbf{h})\mathbf{t}}(x,y,z) = \sum_{q=0}^{q=N-2} e^{-jkqa\sin\varphi_0\sin\theta_0} \underline{\mathbf{E}}^{(\mathbf{h})\mathbf{1}}(x-aq,y,z) \tag{3.49}$$

$$\underline{\mathbf{H}}^{(\mathbf{h})\mathbf{t}}(x,y,z) = \sum_{q=0}^{q=N-2} e^{-jkqa\sin\varphi_0\sin\theta_0} \underline{\mathbf{H}}^{(\mathbf{h})\mathbf{1}}(x-aq,y,z) \tag{3.50}$$

where $\underline{\mathbf{E}}^{(\mathbf{h})\mathbf{1}}(x,y,z)$ and $\underline{\mathbf{H}}^{(\mathbf{h})\mathbf{1}}(x,y,z)$ are the 3-D electric and the 3-D magnetic field between the first two plates $0 \leq x \leq -a$, $-\infty \leq y \leq +\infty$ and $0 \leq z \leq +\infty$, which are found by following the general procedure in (15), and using the total 2-D solution that is obtained by the grid method.

3.4 Array of Four Unequally Spaced Semi-infinite Metal Plates

Figure 21 shows the 2-D geometry of an array consisting of four unequally spaced semi-infinite metal plates with the grid structure. Since there is no characteristic length in the metallic structure in the vertical axis ($y-$axis), there is no limitation in the vertical basic-length (along $y-$axis) of the grid's elements (rectangles). There are three characteristic lengths in the $x-$axis, namely a_1, a_2, and a_3, which make the necessity to apply the condition in Equation 3.51

$$k_x \min(a_1, a_2, a_3) = k \cos\varphi_0 \min(a_1, a_2, a_3) = m\pi, \qquad (m = 0, 1, 2, ...) \tag{3.51}$$

where m non-negative integer is imposed. Only waves 1 and 3 of Figure 1 are needed. The three characteristic lengths a_1, a_2, and a_3 must be commensurable one to another as it is one of the important conditions to construct the grid and apply the grid method. The horizontal basic-length (along $x-$axis) of the grid must equal to the $\min(a_1, a_2, a_3)$ to assure that the obtained GO solutions are the exact solutions to the scattering problem. The wavelength of the incident waves should satisfy the wavelength condition $\lambda \leq 2\min(a_1, a_2, a_3)$. It is important to note that, there are m allowable values for the angle of incidence φ_0, which are

$$\varphi_{0i} = \arccos\left(\frac{i\lambda}{2\min(a_1, a_2, a_3)}\right), \qquad i = 1, 2, ..., m \tag{3.52}$$

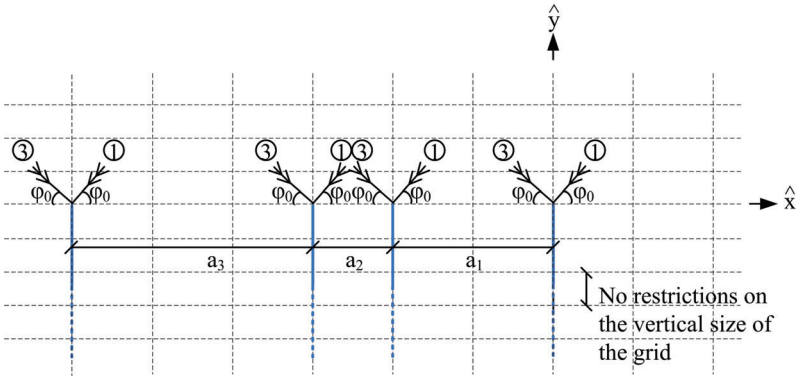

Figure 21. Two-dimensional geometry of an array of four unequally spaced semi-infinite metal plates with the grid structure.

where m is the integer that is used in Equation 3.51 and its maximum allowable value is given by

$$m_{max} \leq \frac{2\min(a_1, a_2, a_3)}{\lambda}. \tag{3.53}$$

3.4.1 Solution to the E-polarization

If all the conditions in the previous section are satisfied, then based on the grid method, the 2-D electric field everywhere is given in Equation 3.19. The corresponding magnetic field follows from Maxwell's equations. The total 3-D electric and magnetic fields are given in Equation 3.20 and Equation 3.21, respectively. It is important to note that there are $N-1$ different TE modes, each individual mode propagates alone in the negative $y-$direction between one of

the $N-1$ two adjacent parallel plates in this metallic structure.

Figure 22 and Figure 23 show the magnitude of the $x-$ and $y-$component of the surface current density on the truncation plate between the four parallel semi-infinite plates for the E-polarization, respectively. The angles of incidence are $\theta_0 = \pi/6$, $\varphi_0 = \pi/3$; while the separation distances between the parallel semi-infinite plates are $a_1 = 2\lambda$, $a_2 = \lambda$ and $a_3 = 3\lambda$.
There are three different modes propagate in the negative $y-$direction. Only one mode propagates between each two adjacent parallel plates.
The $x-$component of the surface current density $J_x^{(e)}$ is perpendicular to the edges, where the parallel plates and truncation plate intersect, hence $J_x^{(e)}$ has its maximum value at these edges; while the $y-$component $J_y^{(e)}$ is parallel to these edges, thus it decays and vanishes at these edges.

3.4.2 Solution to the H-polarization

If all the required conditions are satisfied same as in the E-polarization in the previous section, then and based on the grid method, the 2-D magnetic field everywhere is given by Equation 3.32 and the related 2-D electric field follows from Maxwell's equations. The 3-D electric and magnetic fields are given in Equation 3.33 and Equation 3.34, respectively. There are $N-1$ different TM modes. Each individual mode propagates alone along the negative $y-$direction between one of the $N-1$ two adjacent parallel plates in this metallic structure.

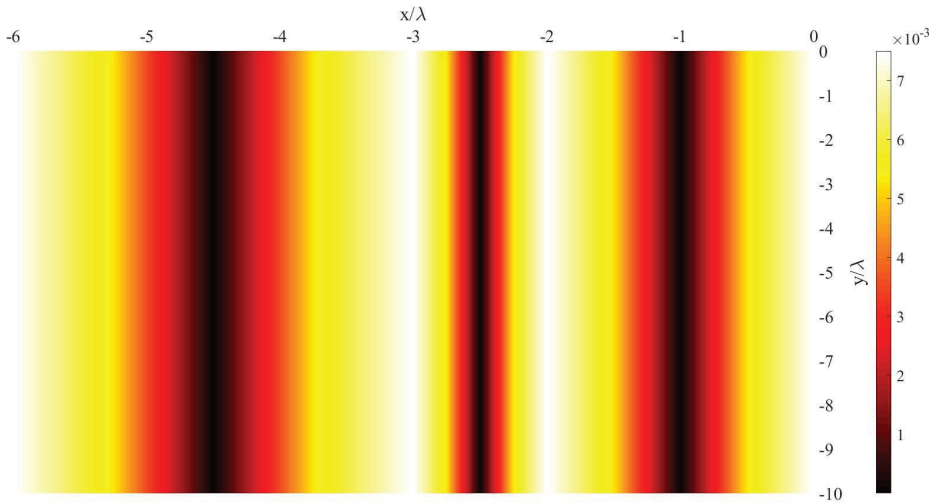

Figure 22. Magnitude of $J_x^{(e)}$ on the truncating plate $z = 0$ between the four parallel semi-infinite plates for E-polarization when $\theta_0 = \pi/6$, $\varphi_0 = \pi/3$, $a_1 = 2\lambda$, $a_2 = \lambda$ and $a_3 = 3\lambda$.

Figure 24 and Figure 25 show the $x-$ and $y-$component of the surface current on the truncation plate for the H-polarization, respectively. It can be seen that the component of the surface current density that is tangential to the edges of the metallic structure (i.e. $J_y^{(h)}$) vanishes at these edges; while the component that is perpendicular to these edges (i.e. $J_x^{(h)}$), has its maximum value at these edges.

3.5 Finite Array of Equally Spaced Thick Semi-infinite Metal Plates

Figure 26 shows 2-D geometry of an array of three equally spaced thick semi-infinite metal plates with the grid structure. This structure belongs to the four-quadrants structures; there-

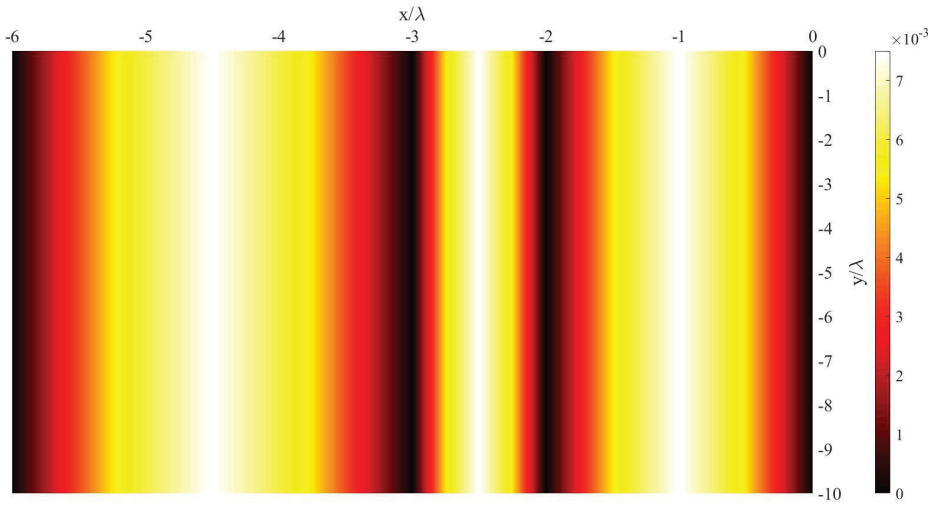

Figure 23. Magnitude of $J_y^{(e)}$ on the truncating plate $z = 0$ between the four parallel semi-infinite plates for E-polarization when $\theta_0 = \pi/6$, $\varphi_0 = \pi/3$, $a_1 = 2\lambda$, $a_2 = \lambda$ and $a_3 = 3\lambda$.

fore, all the four incident plane waves of Figure 1 are needed. There are two characteristic lengths in the horizontal direction in this structure, which are the thickness of the metal plates a_1 and the separation distance a_2. Thus, there is no limitation to choose the vertical basic-length of the grid's elements. The best choice for the horizontal basic-length is given by

$$a = \min(a_1, a_2). \tag{3.54}$$

The two characteristic lengths in the $x-$direction a_1 and a_2 must be commensurable to each other. For the 2-D solution, the condition in Equation 2.11 applies as one of the requirements

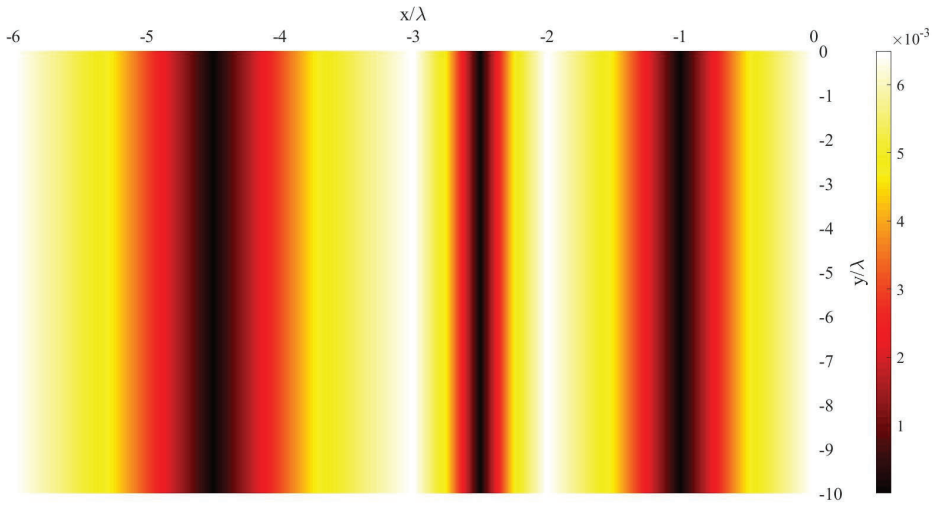

Figure 24. Magnitude of $J_x^{(h)}$ on the truncating plate $z = 0$ between the four parallel semi-infinite plates for H-polarization when $\theta_0 = \pi/6$, $\varphi_0 = \pi/3$, $a_1 = 2\lambda$, $a_2 = \lambda$ and $a_3 = 3\lambda$.

to obtain the exact GO solution. The wavelength of the incident waves should satisfy the condition $\lambda \leq 2a$. There are m possible values for the incidence angle φ_0, which are given in Equation 3.30. The value of m is the the same value that is used in Equation 2.11 and its maximum allowable value is

$$m_{max} \leq \frac{2\min(a_1, a_2)}{\lambda} \tag{3.55}$$

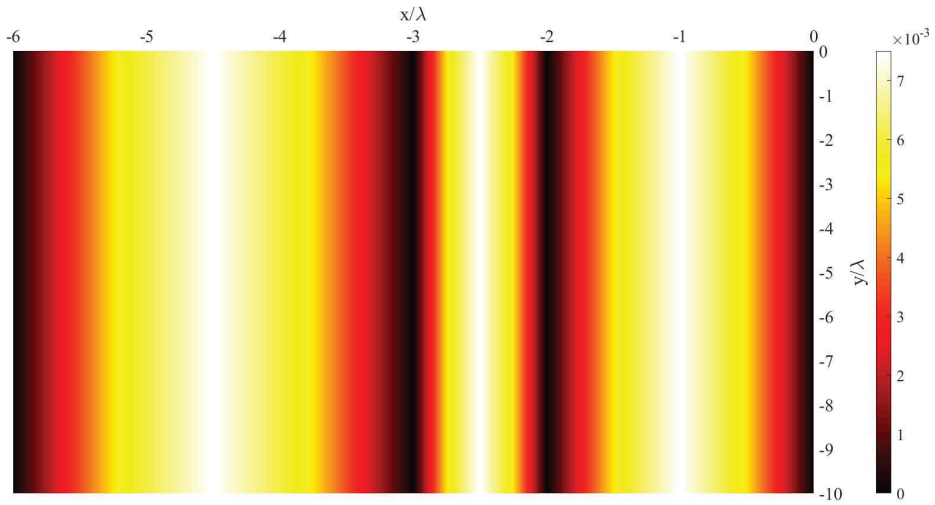

Figure 25. Magnitude of $J_y^{(h)}$ on the truncating plate $z = 0$ between the four parallel semi-infinite plates for H-polarization when $\theta_0 = \pi/6$, $\varphi_0 = \pi/3$, $a_1 = 2\lambda$, $a_2 = \lambda$ and $a_3 = 3\lambda$.

3.5.1 Solution to the E-polarization

Based on the grid method, the total 2-D electric field is given in Equation 2.5. It is the sum of the electric field of the four incident plane waves in Figure 1. The related total 2-D magnetic field follows from Maxwell's equations and it is given in Equation 2.6 and Equation 2.7. There are two TE modes propagate between each two adjacent parallel thick plates. The first mode propagates in the negative $y-$direction, which is a result of the combination of wave 1 and 3 of Figure 1; while wave 2 and 4 combine to generate the second mode, which propagates in the positive $y-$direction.

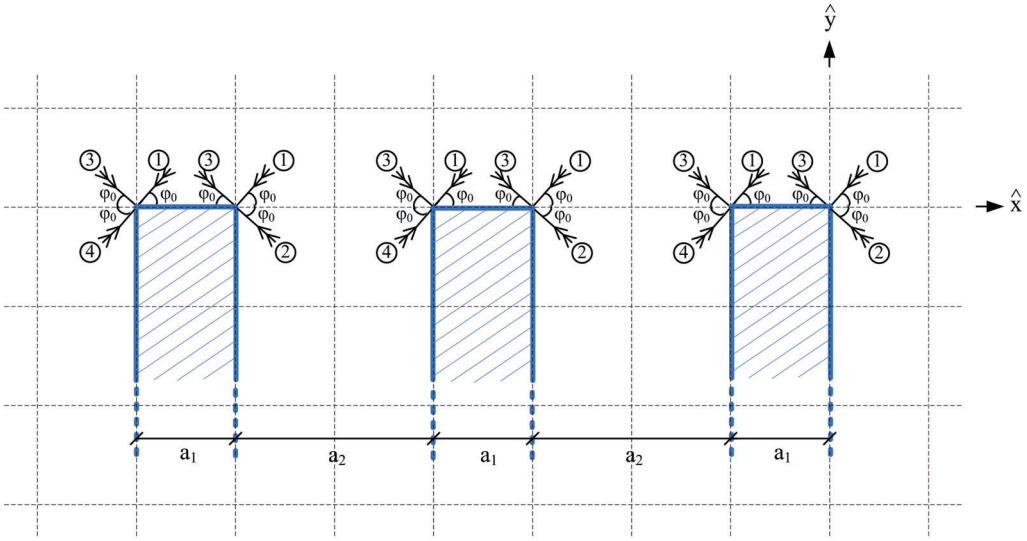

Figure 26. Two-dimensional geometry of an array of three equally spaced thick semi-infinite metal plates with the grid structure.

The 3-D geometry of the problem is shown in Figure 27. The total 3-D solution for oblique incidence when the structure is perpendicularly truncated by a ground plane at $z = 0$ can be obtained by following the procedure in (15), which yields

$$\begin{aligned} U^{(e)}(x, y; k \sin\theta_0) &= 2\left\{\cos[k\rho \sin\theta_0 \cos(\varphi - \varphi_0)] - \cos[k\rho \sin\theta_0 \cos(\varphi + \varphi_0)]\right\} \\ &= -4 \sin(kx \sin\theta_0 \cos\varphi_0) \sin(ky \sin\theta_0 \sin\varphi_0) \\ &= -4 \sin\left(\frac{m\pi}{a} x\right) \sin\left(ky \sin\theta_0 \sin\varphi_0\right) \end{aligned} \tag{3.56}$$

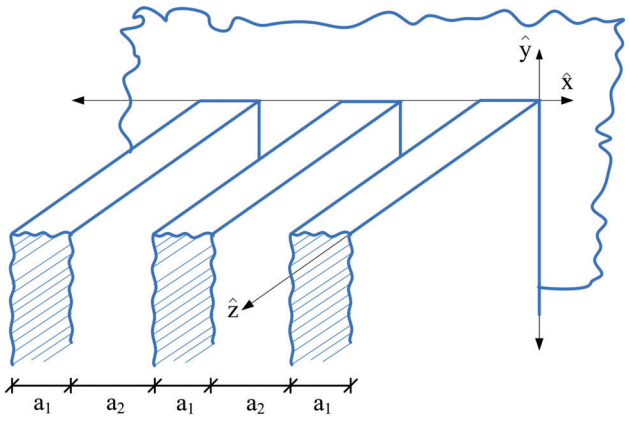

Figure 27. Three-dimensional geometry of an array of three equally spaced thick semi-infinite metal plates truncated perpendicularly by a metal plate at $z = 0$.

$$\begin{aligned}\underline{\mathbf{E}}^{(\mathbf{e})} = 8\cos\theta_0 \sin(kz\cos\theta_0)\Big[&+ \hat{x}\cos\varphi_0 \cos\left(\frac{m\pi}{a}x\right)\sin\left(ky\sin\theta_0\sin\varphi_0\right) \\ &+ \hat{y}\sin\varphi_0 \sin\left(\frac{m\pi}{a}x\right)\cos\left(ky\sin\theta_0\sin\varphi_0\right)\Big] \\ &- \hat{z}8\sin\theta_0\cos(kz\cos\theta_0)\sin\left(\frac{m\pi}{a}x\right)\sin\left(ky\sin\theta_0\sin\varphi_0\right) \end{aligned} \tag{3.57}$$

$$\begin{aligned}\underline{\mathbf{H}}^{(\mathbf{e})} = 8jY\cos(kz\cos\theta_0)\Big[&- \hat{x}\sin\varphi_0 \sin\left(\frac{m\pi}{a}x\right)\cos\left(ky\sin\theta_0\sin\varphi_0\right) \\ &+ \hat{y}\cos\varphi_0 \cos\left(\frac{m\pi}{a}x\right)\sin\left(ky\sin\theta_0\sin\varphi_0\right)\Big] \end{aligned} \tag{3.58}$$

where a is given in Equation 3.54. The condition in Equation 3.59 need to be satisfied in the 3-D geometry

$$ka\sin\theta_0\cos\varphi_0 = m\pi, \tag{3.59}$$

which yields

$$\sin\theta_0 = \frac{m\lambda}{2a\cos\varphi_0}. \tag{3.60}$$

The surface current density $\underline{\mathbf{J}}^{(\mathbf{e})}$ on the truncating plate $z = 0$ is

$$\underline{\mathbf{J}}^{(\mathbf{e})}|_{z=0} = \hat{z} \times \underline{\mathbf{H}}^{(\mathbf{e})} = -8jY\Big[+ \hat{x}\cos\varphi_0 \cos\left(\frac{m\pi}{a}x\right)\sin\left(ky\sin\theta_0\sin\varphi_0\right) + \hat{y}\sin\varphi_0\sin\left(\frac{m\pi}{a}x\right)\cos\left(ky\sin\theta_0\sin\varphi_0\right)\Big]. \tag{3.61}$$

The surface current density $\underline{\mathbf{J}}^{(\mathbf{e})}$ on the upper surfaces of the thick semi-infinite plates $-ja_1-(j-1)a_2 \le x \le (j-1)(-a_1-a_2),\ y = 0$, where j is the number of the thick semi-infinite half-plate ($j = 1, 2, 3, ...$), is given by

$$\underline{\mathbf{J}}^{(\mathbf{e})}|_{y=0} = \hat{y} \times \underline{\mathbf{H}}^{(\mathbf{e})} = \hat{z}8jY\cos(kz\cos\theta_0)\sin\varphi_0\sin\left(\frac{m\pi}{a}x\right). \tag{3.62}$$

The surface current density $\underline{\mathbf{J}}^{(\mathbf{e})}$ on the right-side walls of the thick semi-infinite plates is

$$\underline{\mathbf{J}}^{(\mathbf{e})}|_{\substack{x=0 \\ x=-a_1-a_2 \\ x=-2a_1-2a_2}} = \hat{x} \times \underline{\mathbf{H}}^{(\mathbf{e})} = \hat{z}8jY\eta\cos(kz\cos\theta_0)\cos\varphi_0\sin\left(ky\sin\theta_0\sin\varphi_0\right). \tag{3.63}$$

where η is given by

$$\eta = \begin{cases} 1 & \dfrac{x}{a}\ is\ even \\ (-1)^m & \dfrac{x}{a}\ is\ odd. \end{cases} \tag{3.64}$$

The surface current density $\underline{\mathbf{J}}^{(\mathbf{e})}$ on the left-side walls of the thick semi-infinite plates is

$$\underline{\mathbf{J}}^{(\mathbf{e})}|_{\substack{x=-a_1 \\ x=-2a_1-a_2 \\ x=-3a_1-2a_2}} = -\hat{x} \times \underline{\mathbf{H}}^{(\mathbf{e})} = -\hat{z}8jY\eta \cos(kz\cos\theta_0)\cos\varphi_0 \sin\left(ky\sin\theta_0\sin\varphi_0\right). \tag{3.65}$$

3.5.2 Solution to the H-polarization

The total 2-D magnetic field is given in Equation 2.18. It is the sum of the magnetic field of the four incident plane waves, which are given in Equation 2.14 to Equation 2.17. The total 3-D solution is found based on the procedure in (15)

$$\begin{aligned} U^{(h)}(x,y;k\sin\theta_0) &= 4\cos(kx\sin\theta_0\cos\varphi_0)\cos(ky\sin\theta_0\sin\varphi_0) \\ &= 4\cos\left(\frac{m\pi}{a}x\right)\cos\left(ky\sin\theta_0\sin\varphi_0\right) \end{aligned} \tag{3.66}$$

$$\begin{aligned} \underline{\mathbf{E}}^{(\mathbf{h})} = 8\sin(kz\cos\theta_0)\Big[&-\hat{x}\sin\varphi_0\cos\left(\frac{m\pi}{a}x\right)\sin\left(ky\sin\theta_0\sin\varphi_0\right) \\ &+\hat{y}\cos\varphi_0\sin\left(\frac{m\pi}{a}x\right)\cos\left(ky\sin\theta_0\sin\varphi_0\right)\Big] \end{aligned} \tag{3.67}$$

$$\begin{aligned} \underline{\mathbf{H}}^{(\mathbf{h})} = 8jY\cos\theta_0\cos(kz\cos\theta_0)\Big[&-\hat{x}\cos\varphi_0\sin\left(\frac{m\pi}{a}x\right)\cos\left(ky\sin\theta_0\sin\varphi_0\right) \\ &-\hat{y}\sin\varphi_0\cos\left(\frac{m\pi}{a}x\right)\sin\left(ky\sin\theta_0\sin\varphi_0\right)\Big] \\ &+\hat{z}8jY\sin\theta_0\sin(kz\cos\theta_0)\cos\left(\frac{m\pi}{a}x\right)\cos\left(ky\sin\theta_0\sin\varphi_0\right) \end{aligned} \tag{3.68}$$

where a is given in Equation 3.54 and the condition in Equation 3.59 must be satisfied similar to the E-polarization. The angle of incidence θ_0 is given in Equation 3.60.

The surface current density $\underline{\mathbf{J}}^{(\mathbf{h})}$ on the truncating plate $z = 0$ is

$$\underline{\mathbf{J}}^{(\mathbf{h})}|_{z=0} = \hat{z} \times \underline{\mathbf{H}}^{(\mathbf{h})} = 8jY \cos\theta_0 \Big[+ \hat{x} \sin\varphi_0 \cos\Big(\frac{m\pi}{a}x\Big) \sin\left(ky \sin\theta_0 \sin\varphi_0\right) - \hat{y} \cos\varphi_0 \sin\Big(\frac{m\pi}{a}x\Big) \cos\left(ky \sin\theta_0 \sin\varphi_0\right) \Big]. \tag{3.69}$$

The surface current density $\underline{\mathbf{J}}^{(\mathbf{h})}$ on the upper surfaces of the thick semi-infinite plates $-ja_1 - (j-1)a_2 \leq x \leq (j-1)(-a_1 - a_2),\ y = 0$ is given by

$$\underline{\mathbf{J}}^{(\mathbf{h})}|_{y=0} = \hat{y} \times \underline{\mathbf{H}}^{(\mathbf{h})} = 8jY \Big[+ \hat{x} \sin(kz \cos\theta_0) \sin\theta_0 \cos\Big(\frac{m\pi}{a}x\Big) + \hat{z} \cos\theta_0 \cos\varphi_0 \cos(kz \cos\theta_0) \sin\Big(\frac{m\pi}{a}x\Big) \Big]. \tag{3.70}$$

The surface current density $\underline{\mathbf{J}}^{(\mathbf{h})}$ on the right-side walls of the thick semi-infinite plate is

$$\underline{\mathbf{J}}^{(\mathbf{h})}\Big|_{\substack{x=0 \\ x=-a_1-a_2 \\ x=-2a_1-2a_2 \\ x=-3a_1-2a_2}} = \hat{x} \times \underline{\mathbf{H}}^{(\mathbf{h})} = -8jY\eta \Big[+ \hat{y} \sin\theta_0 \sin(kz \cos\theta_0) \cos\left(ky \sin\theta_0 \sin\varphi_0\right) + \hat{z} \cos\theta_0 \sin\varphi_0 \cos(kz \cos\theta_0) \sin\left(ky \sin\theta_0 \sin\varphi_0\right) \Big]. \tag{3.71}$$

where η is given in Equation 3.64.

The surface current density $\underline{\mathbf{J}}^{(\mathbf{h})}$ on the left-side walls of the thick semi-infinite plate is

$$\underline{\mathbf{J}}^{(\mathbf{h})}|_{\substack{x=-a_1 \\ x=-2a_1-a_2 \\ x=-3a_1-2a_2}} = -\hat{x} \times \underline{\mathbf{H}}^{(\mathbf{h})} = 8jY\eta\Big[+ \hat{y}\sin\theta_0 \sin(kz\cos\theta_0)\cos(ky\sin\theta_0\sin\varphi_0) + \hat{z}\cos\theta_0\sin\varphi_0\cos(kz\cos\theta_0)\sin(ky\sin\theta_0\sin\varphi_0)\Big]. \tag{3.72}$$

3.6 Truncated Metal Grating

The scattering of multiple incident plane waves by planar metallic grating truncated by a metal plane oriented perpendicular to the grooves or ridges of the grating is discussed in this section. The grating may be of either finite or infinite extent in the direction perpendicular to the ridges (Figure 28) or grooves (Figure 29) , i.e. it may consist of either a finite or an infinite number of grooves or ridges. As in the other structures, which were discussed previously, the exact analytical solution to the electromagnetic boundary-value problem is obtained in two steps. First, the two-dimensional problem of a grating of infinite length in the direction of the grooves or ridges on which the primary plane waves are incident perpendicularly to the edges of the grooves or ridges is considered. Once the 2-D solution is obtained, it is extended to oblique incidence with respect to the direction of the grooves or ridges, and to truncation by a metal plane perpendicular to the grooves or ridges, by utilizing the general method in (15).

The ridges (Figure 28) and the grooves (Figure 29) belong to the two-quadrant structures; therefore, only wave 1 and wave 3 of Figure 1 are required, the other waves 2 and 4 being

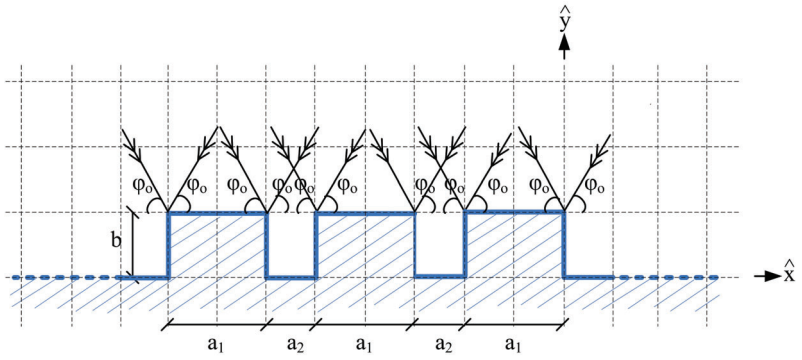

Figure 28. Two-dimensional geometry of three ridges on a metal plate.

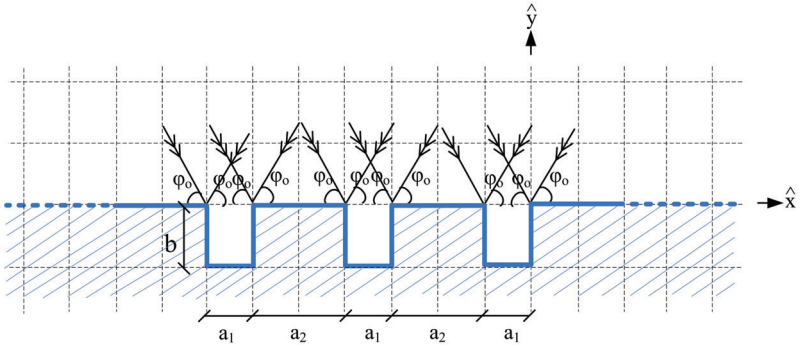

Figure 29. Two-dimensional geometry of three grooves on a metal plate.

reflections of waves 1 and 3 on the metal walls. In the 2-D solution of the problem, both conditions in Equation 2.11 and Equation 2.12 need to be applied to get the exact GO solutions, where a is given in Equation 3.54.

The two characteristic lengths a_1 and a_2 have to be commensurable to each other. Since the characteristic lengths exist in the horizontal and the vertical axis, there will be limitation in the horizontal and the vertical basic-lengths of the rectangles (grid's elements). The vertical basic-length of the rectangles must equal to smallest characteristic length in the vertical direction, which is b; while the horizontal basic-length of the rectangles need to be equal to the smallest characteristic length in the horizontal axis. Since there are two characteristic lengths along $x-$axis, which are a_1 and a_2, then the horizontal basic-length of the rectangles equals to the smallest value of a_1 and a_2, which is given in Equation 3.54. The wavelength of the incident waves is given in Equation 2.25, and it must satisfy the condition in Equation 3.73

$$\lambda \leq 2\min(a_1, a_2, b). \tag{3.73}$$

There are more than one possible value for the angle of incidence φ_0, which are given in Equation 3.30 and Equation 3.31.

3.6.1 Solution to the E-polarization

The two-dimensional geometry of the ridges and grooves structures are shown in Figure 28 and Figure 29, respectively. Only two plane waves of Figure 1 are required, which are waves

1 and 3. Based on the grid method, the total 2-D field for the E-polarization is given in Equation 2.5. The related total 2-D magnetic field is given in Equation 2.6 and Equation 2.7.

The 3-D geometry of the truncated metallic grating is shown in Figure 30, the total 3-D solution for oblique incidence when the structure is perpendicularly truncated by a ground plane at $z = 0$, can be obtained by following the procedure in (15), which yields

$$\begin{aligned} U^{(e)}(x, y; \gamma) &= 2\left\{\cos[\gamma\rho\cos(\varphi - \varphi_0)] - \cos[\gamma\rho\cos(\varphi + \varphi_0)]\right\} \\ &= -4\sin(\gamma x\cos\varphi_0)\sin(\gamma y\sin\varphi_0) \\ &= -4\sin\left(\frac{m\pi}{a}x\right)\sin\left(\frac{n\pi}{b}y\right) \end{aligned} \tag{3.74}$$

$$\begin{aligned} \underline{\mathbf{E}}^{(\mathbf{e})} &= 4\cos\theta_0\sin(kz\cos\theta_0)\times \\ &\quad (\hat{\rho}\{\sin[\gamma\rho\cos(\varphi - \varphi_0)]\cos(\varphi - \varphi_0) - \sin[\gamma\rho\cos(\varphi + \varphi_0)]\cos(\varphi + \varphi_0)\} \\ &\quad - \hat{\varphi}\{\sin[\gamma\rho\cos(\varphi - \varphi_0)]\sin(\varphi - \varphi_0) - \sin[\gamma\rho\cos(\varphi + \varphi_0)]\sin(\varphi + \varphi_0)\}) \\ &\quad + \hat{z}4\sin\theta_0\cos(kz\cos\theta_0)\{\cos[\gamma\rho\cos(\varphi - \varphi_0)] - \cos[\gamma\rho\cos(\varphi + \varphi_0)]\} \\ &= 8\cos\theta_0\sin(kz\cos\theta_0)\Big[\hat{x}\cos\varphi_0\cos\left(\frac{m\pi}{a}x\right)\sin\left(\frac{n\pi}{b}y\right) \\ &\quad + \hat{y}\sin\varphi_0\sin\left(\frac{m\pi}{a}x\right)\cos\left(\frac{n\pi}{b}y\right)\Big] \\ &\quad - \hat{z}8\sin\theta_0\cos(kz\cos\theta_0)\sin\left(\frac{m\pi}{a}x\right)\sin\left(\frac{n\pi}{b}y\right) \end{aligned} \tag{3.75}$$

$$\begin{aligned}\underline{\mathbf{H}}^{(\mathbf{e})} &= 4jY\cos(kz\cos\theta_0)\times \\ &\quad (\hat{\rho}\{\sin[\gamma\rho\cos(\varphi-\varphi_0)]\sin(\varphi-\varphi_0)-\sin[\gamma\rho\cos(\varphi+\varphi_0)]\sin(\varphi+\varphi_0)\} \\ &\quad +\hat{\varphi}\{\sin[\gamma\rho\cos(\varphi-\varphi_0)]\cos(\varphi-\varphi_0)-\sin[\gamma\rho\cos(\varphi+\varphi_0)]\cos(\varphi+\varphi_0)\}) \\ &= 8jY\cos(kz\cos\theta_0)\Big[-\hat{x}\sin\varphi_0\sin\Big(\frac{m\pi}{a}x\Big)\cos\Big(\frac{n\pi}{b}y\Big) \\ &\quad +\hat{y}\cos\varphi_0\cos\Big(\frac{m\pi}{a}x\Big)\sin\Big(\frac{n\pi}{b}y\Big)\Big] \end{aligned} \tag{3.76}$$

where γ is given by

$$\gamma = k\sin\theta_0 \tag{3.77}$$

and a is given in Equation 3.54. In the three-dimensional solution of the problem, the condition in Equation 3.78 in addition to the condition in Equation 3.59 need to be satisfied

$$kb\sin\theta_0\sin\varphi_0 = n\pi. \tag{3.78}$$

From Equation 3.59 and Equation 3.78, the following relations related to the incidence angles φ_0 and θ_0 can be obtained

$$\cos\varphi_0 = \frac{\frac{m}{a}}{\sqrt{\left(\frac{m}{a}\right)^2+\left(\frac{n}{b}\right)^2}} \tag{3.79}$$

$$\sin\varphi_0 = \frac{\frac{n}{b}}{\sqrt{\left(\frac{m}{a}\right)^2+\left(\frac{n}{b}\right)^2}} \tag{3.80}$$

$$\sin\theta_0 = \frac{\pi}{k}\sqrt{\left(\frac{m}{a}\right)^2+\left(\frac{n}{b}\right)^2}. \tag{3.81}$$

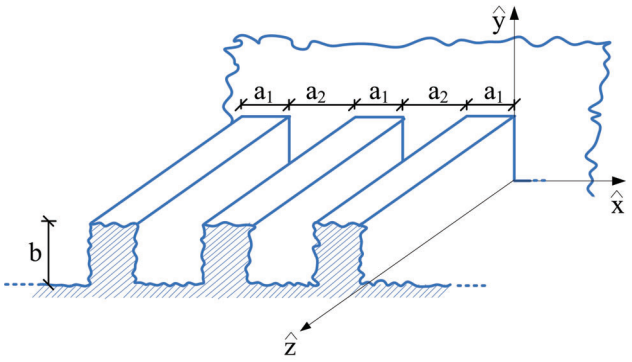

Figure 30. Tree-dimensional geometry of the truncated metallic grating.

The surface current density on the truncating plate $z = 0$ is

$$\underline{\mathbf{J}}^{(\mathbf{e})}|_{z=0} = \hat{z} \times \underline{\mathbf{H}}^{(\mathbf{e})} = 8jY\Big[-\hat{x}\cos\varphi_0 \cos\Big(\frac{m\pi}{a}x\Big)\sin\Big(\frac{n\pi}{b}y\Big) - \hat{y}\sin\varphi_0 \sin\Big(\frac{m\pi}{a}x\Big)\cos\Big(\frac{n\pi}{b}y\Big)\Big]. \tag{3.82}$$

The surface current density on the upper plates of the ridges in the grating $-ja_1-(j-1)a_2 \le x \le (j-1)(-a_1-a_2),\ y = b$, where j is the number of the ridge $(j = 1, 2, 3, ...)$, is given by

$$\underline{\mathbf{J}}^{(\mathbf{e})}|_{y=b} = \hat{y} \times \underline{\mathbf{H}}^{(\mathbf{e})} = \hat{z}(-1)^n 8jY\cos(kz\cos\theta_0)\sin\varphi_0 \sin\Big(\frac{m\pi}{a}x\Big). \tag{3.83}$$

The surface current density on the bottom plates of the grating $j(-a_1 - a_2) \leq x \leq -ja_1 - (j-1)a_2,\ y = 0$ is given by

$$\underline{\mathbf{J}}^{(\mathbf{e})}|_{y=0} = \hat{y} \times \underline{\mathbf{H}}^{(\mathbf{e})} = \hat{z}8jY \cos(kz\cos\theta_0)\sin\varphi_0 \sin\left(\frac{m\pi}{a}x\right). \tag{3.84}$$

The surface current density on the right-side walls $x = (j-1)(-a_1 - a_2)$ in the grating is given by

$$\underline{\mathbf{J}}^{(\mathbf{e})}|_{x=0,-a_1-a_2,-2a_1-2a_2,\ldots} = \hat{x} \times \underline{\mathbf{H}}^{(\mathbf{e})} = \hat{z}8jY\eta \cos(kz\cos\theta_0)\cos\varphi_0 \sin\left(\frac{n\pi}{b}y\right) \tag{3.85}$$

where η is given in Equation 3.64.

The surface current density on the left-side walls $x = -ja_1 + (j-1)(-a_1 - a_2)$ in the grating is given by

$$\underline{\mathbf{J}}^{(\mathbf{e})}|_{x=-a_1,-2a_1-a_2,\ldots} = -\hat{x} \times \underline{\mathbf{H}}^{(\mathbf{e})} = -\hat{z}8jY\eta \cos(kz\cos\theta_0)\cos\varphi_0 \sin\left(\frac{n\pi}{b}y\right). \tag{3.86}$$

3.6.2 Solution to the H-polarization

The total 2-D magnetic field is given in Equation 2.18. It is the sum of the magnetic field of the four incident plane waves, which are given in Equation 2.14 to Equation 2.17. The related

total 2-D electric field is given in Equation 2.19 and Equation 2.20. The total 3-D solution for oblique incidence is found based on the procedure in (15)

$$\begin{aligned} U^{(h)}(x,y;k\sin\theta_0) &= 4\cos(kx\sin\theta_0\cos\varphi_0)\cos(ky\sin\theta_0\sin\varphi_0) \\ &= 4\cos\Big(\frac{m\pi}{a}x\Big)\cos\Big(\frac{n\pi}{b}y\Big) \end{aligned} \tag{3.87}$$

$$\begin{aligned} \underline{\mathbf{E}}^{(\mathbf{h})} = 8\sin(kz\cos\theta_0)\Big[&-\hat{x}\sin\varphi_0\cos\Big(\frac{m\pi}{a}x\Big)\sin\Big(\frac{n\pi}{b}y\Big) \\ &+\hat{y}\cos\varphi_0\sin\Big(\frac{m\pi}{a}x\Big)\cos\Big(\frac{n\pi}{b}y\Big)\Big] \end{aligned} \tag{3.88}$$

$$\begin{aligned} \underline{\mathbf{H}}^{(\mathbf{h})} = 8jY\cos\theta_0\cos(kz\cos\theta_0)\Big[&-\hat{x}\cos\varphi_0\sin\Big(\frac{m\pi}{a}x\Big)\cos\Big(\frac{n\pi}{b}y\Big) \\ &-\hat{y}\sin\varphi_0\cos\Big(\frac{m\pi}{a}x\Big)\sin\Big(\frac{n\pi}{b}y\Big)\Big] \\ &+\hat{z}8jY\sin\theta_0\sin(kz\cos\theta_0)\cos\Big(\frac{m\pi}{a}x\Big)\cos\Big(\frac{n\pi}{b}y\Big) \end{aligned} \tag{3.89}$$

where a is given in Equation 3.54. Similar to the E-polarization, the conditions in Equation 3.59 and Equation 3.78 apply. The angle of incidence θ_0 is given in Equation 3.81.

The surface current density $\underline{\mathbf{J}}^{(\mathbf{h})}$ on the truncating plate $z = 0$ is

$$\begin{aligned} \underline{\mathbf{J}}^{(\mathbf{h})}|_{z=0} = \hat{z}\times\underline{\mathbf{H}}^{(\mathbf{h})} = 8jY\cos\theta_0\Big[&+\hat{x}\sin\varphi_0\cos\Big(\frac{m\pi}{a}x\Big)\sin\Big(\frac{n\pi}{b}y\Big) \\ &-\hat{y}\cos\varphi_0\sin\Big(\frac{m\pi}{a}x\Big)\cos\Big(\frac{n\pi}{b}y\Big)\Big]. \end{aligned} \tag{3.90}$$

The surface current density on the upper plates $-ja_1-(j-1)a_2 \le x \le (j-1)(-a_1-a_2),\ y=b$ of the ridges in the grating is given by

$$\underline{\mathbf{J}}^{(\mathbf{h})}|_{y=b} = \hat{y} \times \underline{\mathbf{H}}^{(\mathbf{h})} = 8jY(-1)^n \Big[+ \hat{x} \sin\theta_0 \sin(kz\cos\theta_0) \cos\Big(\frac{m\pi}{a}x\Big) + \hat{z} \cos\theta_0 \cos(kz\cos\theta_0) \cos\varphi_0 \sin\Big(\frac{m\pi}{a}x\Big) \Big]. \tag{3.91}$$

The surface current density on the bottom plates $j(-a_1-a_2) \le x \le -ja_1-(j-1)a_2,\ y=0$ in grating is

$$\underline{\mathbf{J}}^{(\mathbf{h})}|_{y=0} = \hat{y} \times \underline{\mathbf{H}}^{(\mathbf{h})} = 8jY \Big[+ \hat{x} \sin\theta_0 \sin(kz\cos\theta_0) \cos\Big(\frac{m\pi}{a}x\Big) + \hat{z} \cos\theta_0 \cos(kz\cos\theta_0) \cos\varphi_0 \sin\Big(\frac{m\pi}{a}x\Big) \Big]. \tag{3.92}$$

The surface current density on the right-side walls $x=(j-1)(-a_1-a_2)$ in the grating is

$$\underline{\mathbf{J}}^{(\mathbf{h})}|_{x=0,-a_1-a_2,-2a_1-2a_2,\ldots} = \hat{x} \times \underline{\mathbf{H}}^{(\mathbf{h})} = -8jY\eta \Big[+ \hat{y} \sin\theta_0 \sin(kz\cos\theta_0) \cos\Big(\frac{n\pi}{b}y\Big) + \hat{z} \cos\theta_0 \cos(kz\cos\theta_0) \sin\varphi_0 \sin\Big(\frac{n\pi}{b}y\Big) \Big] \tag{3.93}$$

where η is given inEquation 3.64.

The surface current density on the left-side walls $x = -ja_1 + (j-1)(-a_1 - a_2)$ in the grating is

$$\underline{\mathbf{J}}^{(\mathbf{h})}|_{x=-a_1,-2a_1-a_2,\ldots} = -\hat{x} \times \underline{\mathbf{H}}^{(\mathbf{h})} = 8jY\eta\Big[+ \hat{y}\sin\theta_0 \sin(kz\cos\theta_0)\cos\Big(\frac{n\pi}{b}y\Big) + \hat{z}\cos\theta_0\cos(kz\cos\theta_0)\sin\varphi_0\sin\Big(\frac{n\pi}{b}y\Big)\Big]. \quad (3.94)$$

3.7 Single Rectangular Pillar

The solution to the scattering of multiple incident plane waves by a single rectangular cross-section pillar is developed in two-dimensions with normal incidence. Then, the obtained 2-D solution is generalized to the 3-D solution based on the procedure in (15). The metallic pillar structure is assumed to be made of perfect electric conductor material, and is immersed in a lossless, homogeneous and isotropic medium such as free space. The two-dimensional geometry of the problem is shown in Figure 31. Similar structure was previously studied in (29). The pillar structure belongs to the four-quadrant structures; therefore, all the four incident plane waves of Figure 1 are needed, in addition to satisfy certain conditions (discussed herein) needed to obtain the exact GO solutions to the scattering problem.

There are two characteristic lengths in the pillar structure, which are the pillar dimensions a and b in the horizontal and vertical axis, respectively. To construct the grid, the best dimensions for the horizontal and vertical basic-length of the grid's elements (rectangles) are to be equal the pillar dimensions in the horizontal a and vertical b axis, respectively.

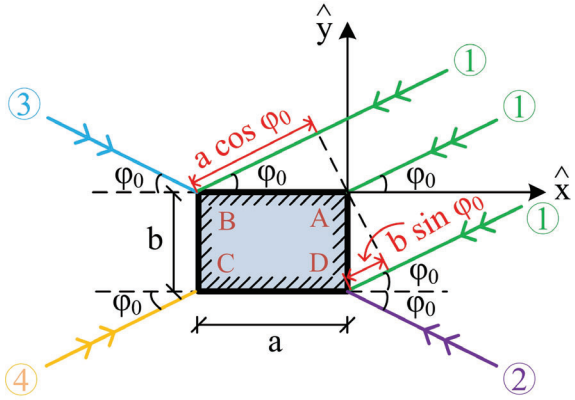

Figure 31. Two-dimensional geometry of single rectangular pillar structure.

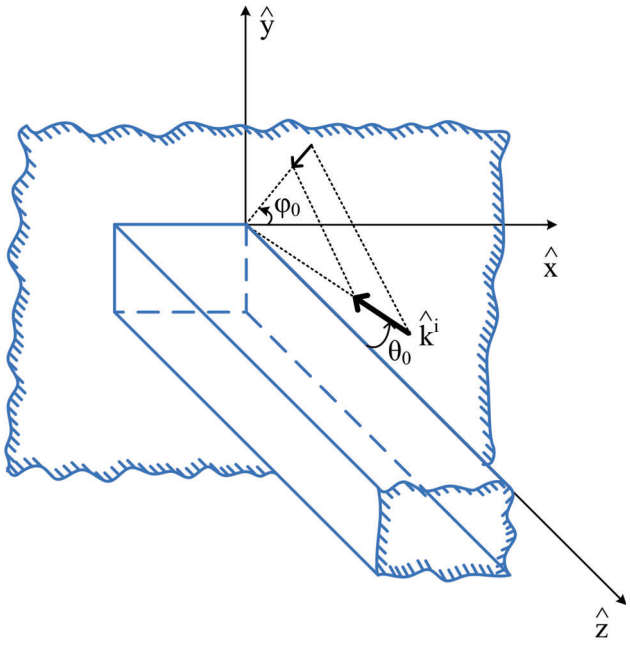

Figure 32. Three-dimensional geometry of a truncated rectangular pillar.

3.7.1 Solution to the E-polarization

The electric fields of the four required incident plane waves in two-dimensional geometry are given in Equation 2.1 to Equation 2.4. Based on the grid method, the sum of the electric field of these plane waves gives the total 2-D electric field, which is given in Equation 2.5. The corresponding total 2-D magnetic field can be found from Maxwell's equations, which is given in Equation 2.6 to Equation 2.7.

It is obvious from Figure 31 that, there is a delay of $a\cos\varphi_0$ for the incident wave 1 to reach edge B compared to edge A. Also, there is a delay of $b\sin\varphi_0$ for the incident wave 1 to reach edge D compared to edge A. These delay values must be equal to the half wavelength of the incident plane waves or its multiplication, thus

$$a\cos\varphi_0 = m\frac{\lambda}{2} \tag{3.95}$$

$$\cos\varphi_0 = \frac{m\lambda}{2a} \tag{3.96}$$

$$b\sin\varphi_0 = n\frac{\lambda}{2} \tag{3.97}$$

$$\sin\varphi_0 = \frac{n\lambda}{2b} \tag{3.98}$$

where m and n are positive integers. By using similar analysis, the same delay can be found associates with the other three incident plane waves. The relations in Equation 3.96 and Equation 3.98 lead to the fundamental relation in Equation 2.24, which represents one of the conditions that must be satisfied in order to obtain the exact GO solutions to the boundary-value problem. Also, both wavelength conditions in Equation 2.27 need to be satisfied. There

are more than one possible values for the angle of incidence φ_0, which are given in Equation 2.30 and Equation 2.31. Basically, it depends on the wavelength, the dimensions of the pillar (a and b), and the values of the integers (m and n).

The obtained 2-D solution in Equation 2.5 is generalized to 3-D solution for oblique incidence case when the rectangular pillar is perpendicularly truncated by a metallic ground plate at $z = 0$, and the pillar extends indefinitely in the positive $z-$direction. The 3-D geometry of the problem is shown in Figure 32. The direction of propagation of the primary incident wave 1 forms the angle θ_0 with the negative $z-$axis; while its projection on the xy plane forms the angle φ_0 with the negative $x-$axis. The direction of propagation of the four incident plane waves are given in Equation 3.1 to Equation 3.4. The 3-D electric field of the four incident plane waves are given in Equation 3.5 to Equation 3.8, while the corresponding magnetic fields can be found by Maxwell's equations. The total 3-D solution is given in Equation 3.75 and Equation 3.76, which is obtain by following the procedure in (15). The conditions given in Equation 3.59 and Equation 3.78 need to be applied in the 3-D solution of the problem. The incidence angle θ_0 is given in Equation 3.81.

The surface current density $\underline{\mathbf{J}}^{(\mathbf{e})}$ on the truncating plane $z = 0$ is given in Equation 3.82. The surface current density on the upper surface of the pillar $-a \leq x \leq 0,\ y = 0$ is given by

$$\underline{\mathbf{J}}^{(\mathbf{e})}|_{y=0} = \hat{y} \times \underline{\mathbf{H}}^{(\mathbf{e})} = \hat{z} 8jY \cos(kz \cos\theta_0) \sin\varphi_0 \sin\left(\frac{m\pi}{a}x\right). \tag{3.99}$$

The surface current density on the bottom surface of the pillar $-a \leq x \leq 0,\ y = -b$ is given by

$$\underline{\mathbf{J}}^{(\mathbf{e})}|_{y=-b} = -\hat{y} \times \underline{\mathbf{H}}^{(\mathbf{e})} = -\hat{z}(-1)^n 8jY \cos(kz\cos\theta_0)\sin\varphi_0 \sin\left(\frac{m\pi}{a}x\right). \tag{3.100}$$

The surface current density $\underline{\mathbf{J}}^{(\mathbf{e})}$ on the right-side plate of the pillar $x = 0,\ -b \leq y \leq 0$ is

$$\underline{\mathbf{J}}^{(\mathbf{e})}|_{x=0} = \hat{x} \times \underline{\mathbf{H}}^{(\mathbf{e})} = \hat{z} 8jY \cos(kz\cos\theta_0)\cos\varphi_0 \sin\left(\frac{n\pi}{b}y\right). \tag{3.101}$$

The surface current density $\underline{\mathbf{J}}^{(\mathbf{e})}$ on the left-side plate of the pillar $x = -a,\ -b \leq y \leq 0$ is

$$\underline{\mathbf{J}}^{(\mathbf{e})}|_{x=-a} = -\hat{x} \times \underline{\mathbf{H}}^{(\mathbf{e})} = -\hat{z} 8jY(-1)^m \cos(kz\cos\theta_0)\cos\varphi_0 \sin\left(\frac{n\pi}{b}y\right). \tag{3.102}$$

3.7.2 Solution to the H-polarization

The total 2-D magnetic field is given in Equation 2.18, which is the sum of the magnetic field of the four incident plane waves, which are given in Equation 2.14 to Equation 2.17. The related total 2-D electric field is given in Equation 2.19 and Equation 2.20. The total 3-D solution for oblique incidence is found based on the procedure in (15), which is given in Equation 3.88 and Equation 3.89. As in the case of E-polarization, the conditions given in Equation 3.59 and Equation 3.78 apply, and the incidence angle θ_0 is given in Equation 3.81.

The surface current density $\underline{\mathbf{J}}^{(\mathbf{h})}$ on the truncating plane $z = 0$, is given in Equation 3.90. The surface current density on the upper surface of the pillar $-a \leq x \leq 0,\ y = 0$ is

$$\underline{\mathbf{J}}^{(\mathbf{h})}|_{y=0} = \hat{y} \times \underline{\mathbf{H}}^{(\mathbf{h})} = 8jY\Big[+ \hat{x} \sin\theta_0 \sin(kz\cos\theta_0) \cos\Big(\frac{m\pi}{a}x\Big) + \hat{z} \cos\theta_0 \cos(kz\cos\theta_0) \cos\varphi_0 \sin\Big(\frac{m\pi}{a}x\Big)\Big]. \tag{3.103}$$

The surface current density on the bottom surface of the pillar $-a \leq x \leq 0,\ y = -b$ is

$$\underline{\mathbf{J}}^{(\mathbf{h})}|_{y=-b} = -\hat{y} \times \underline{\mathbf{H}}^{(\mathbf{h})} = -8jY(-1)^n\Big[+ \hat{x} \sin\theta_0 \sin(kz\cos\theta_0) \cos\Big(\frac{m\pi}{a}x\Big) + \hat{z} \cos\theta_0 \cos(kz\cos\theta_0) \cos\varphi_0 \sin\Big(\frac{m\pi}{a}x\Big)\Big]. \tag{3.104}$$

The surface current density $\underline{\mathbf{J}}^{(\mathbf{h})}$ on the right-side plate of the pillar $x = 0,\ -b \leq y \leq 0$ is

$$\underline{\mathbf{J}}^{(\mathbf{h})}|_{x=0} = \hat{x} \times \underline{\mathbf{H}}^{(\mathbf{h})} = -8jY\Big[+ \hat{y} \sin\theta_0 \sin(kz\cos\theta_0) \cos\Big(\frac{n\pi}{b}y\Big) + \hat{z} \cos\theta_0 \cos(kz\cos\theta_0) \sin\varphi_0 \sin\Big(\frac{n\pi}{b}y\Big)\Big]. \tag{3.105}$$

The surface current density $\underline{\mathbf{J}}^{(\mathbf{h})}$ on the left-side plate of the pillar $x = -a,\ -b \leq y \leq 0$ is

$$\underline{\mathbf{J}}^{(\mathbf{h})}|_{x=-a} = -\hat{x} \times \underline{\mathbf{H}}^{(\mathbf{h})} = 8jY(-1)^m\Big[+ \hat{y} \sin\theta_0 \sin(kz\cos\theta_0) \cos\Big(\frac{n\pi}{b}y\Big) + \hat{z} \cos\theta_0 \cos(kz\cos\theta_0) \sin\varphi_0 \sin\Big(\frac{n\pi}{b}y\Big)\Big]. \tag{3.106}$$

The surface current density on the upper plate of the pillar ($-\lambda \leq x \leq 0,\ y = 0,\ 10\lambda \leq z \leq 0$) is shown in Figure 33 for the E-polarization, when the angles of incidence $\theta_0 = \pi/6$, $\varphi_0 = \pi/3$, pillar side-width $a = 1\lambda$ and for 10λ along the positive $z-$direction. The surface current density has only one component, which is in the $z-$direction. $J_z^{(e)}$ is parallel to the edges of the pillar along the $z-$axis, thus the surface current density decays and becomes zero at these edges. At the same time, $J_z^{(e)}$ is perpendicular to the truncation plate, thus $J_z^{(e)}$ has a maximum value at the intersection of the truncation plate and the pillar as $J_z^{(e)}$ moves towards the truncation plate to avoid charge accumulation at the edges. There is no mode that propagates in the $z-$direction as it can be seen in Figure 33.

Figure 34 and Figure 35 show the $x-$ and $z-$component of the surface current density on the upper plate of the pillar for the H-polarization, respectively. Again, it can be seen that the perpendicular component $J_x^{(h)}$ has a maximum value at the edges and is perpendicular to them; while the parallel component $J_z^{(h}$ is zero at the edges and is parallel with them.

Figure 36 shows the only component of the surface current density on the right-side plate of the pillar for the E-polarization, which is in the $z-$direction. Figure 37 and Figure 38 show the $y-$ and $z-$component of the surface current density on the right-side plate for the H-polarization case, respectively. All the components of the surface current densities that are perpendicular to the edges satisfy the continuity conditions across these edges; while all the parallel components vanish across these edges as it can be seen in the related figures.

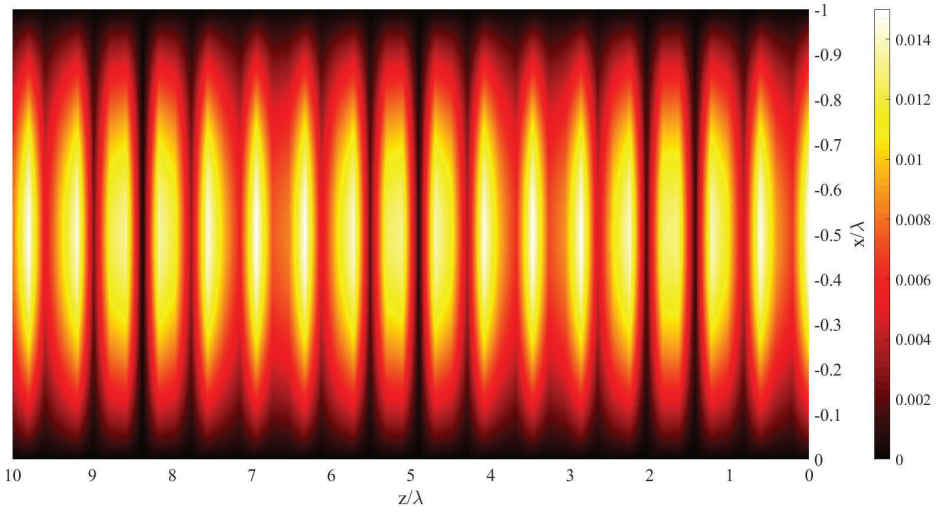

Figure 33. Magnitude of $J_z^{(e)}$ on the upper plate of the pillar $(-\lambda \leq x \leq 0,\ y = 0,\ 10\lambda \leq z \leq 0)$ when $\theta_0 = \pi/6$, $\varphi_0 = \pi/3$, and $a = 1\lambda$.

3.8 Array of Rectangular Pillars

The exact GO solution to the scattering by an array of finite (or infinite) number of rectangular cylinders under multiple plane waves excitation is developed. The pillars (cylinders) are equally spaced, infinitely long, and rectangular cross-section. The separation distance between each two adjacent pillars is a_2. The structure belongs to the four-quadrant structures; therefore, all the four incident plane waves of Figure 1 are needed to obtain the exact GO solutions. Figure 39 shows the 2-D geometry of an array consists of three rectangular cross-section pillars with the grid structure, the dimensions of the pillars are a_1 and b in the horizontal and vertical axis, respectively. The two horizontal characteristic lengths in the structure a_1, and a_2 must

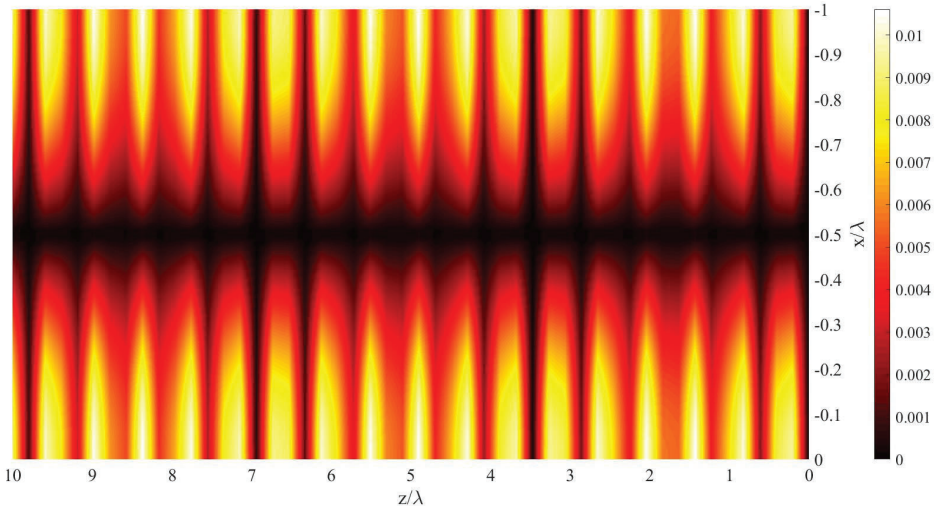

Figure 34. Magnitude of $J_x^{(h)}$ on the upper plate of the pillar $(-\lambda \leq x \leq 0,\ y = 0,\ 10\lambda \leq z \leq 0)$ when $\theta_0 = \pi/6$, $\varphi_0 = \pi/3$, and $a = 1\lambda$.

be commensurable one to another. To construct the grid, since there is only one characteristic length in the $y-$direction, the best choice for the vertical basic-length of the rectangles (elements of the grid) is b; while the best horizontal basic-length of the rectangles (i.e. along the $x-$axis) is given in Equation 3.54.

The wavelength condition $\lambda \leq \min(a_1, b, a_2)$, in addition to the conditions in Equation 2.11 and Equation 2.12 should be satisfied. There are m or n values of the angle of incidence φ_0, which can be obtained by Equation 3.30 and Equation 3.31, where m and n are the integers that are used in Equation 2.11 and Equation 2.12.

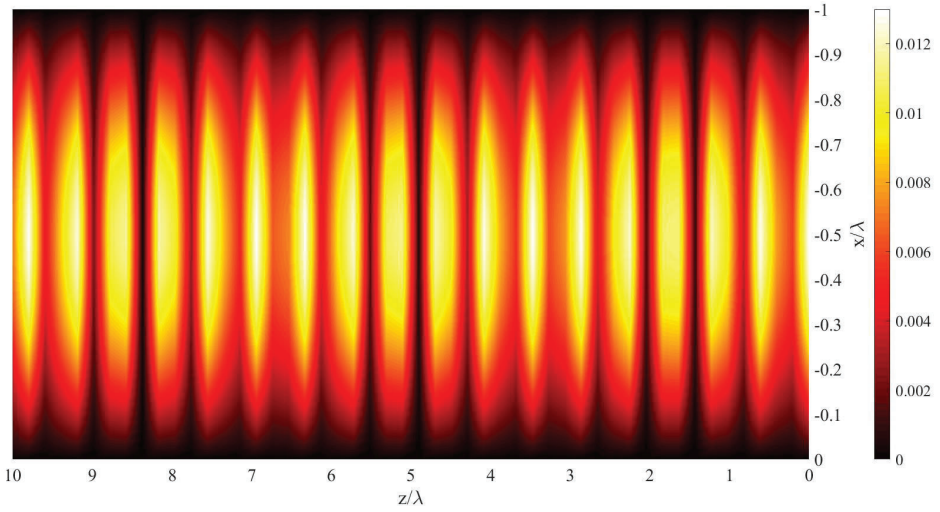

Figure 35. Magnitude of $J_z^{(h)}$ on the upper plate of the pillar $(-\lambda \leq x \leq 0,\ y = 0,\ 10\lambda \leq z \leq 0)$ when $\theta_0 = \pi/6$, $\varphi_0 = \pi/3$, and $a = 1\lambda$.

3.8.1 Solution to the E-polarization

In the two-dimensional geometry, the array structure is illuminated by four incident plane waves, which are given in Equation 2.1 to Equation 2.4 similar to the case of the single pillar structure. The total 2-D electric field is given in Equation 2.5, which is the sum of the electric field of the four incident plane waves. The related total 2-D magnetic field follows from Maxwell's equations and it is given in Equation 2.6 and Equation 2.7.

The obtained 2-D solution is extended to 3-D solution for oblique incidence when the rectangular pillars are perpendicularly truncated by a metallic ground plate at $z = 0$, and the pillars extend indefinitely in the positive $z-$direction by following the procedure in (15). The 3-D

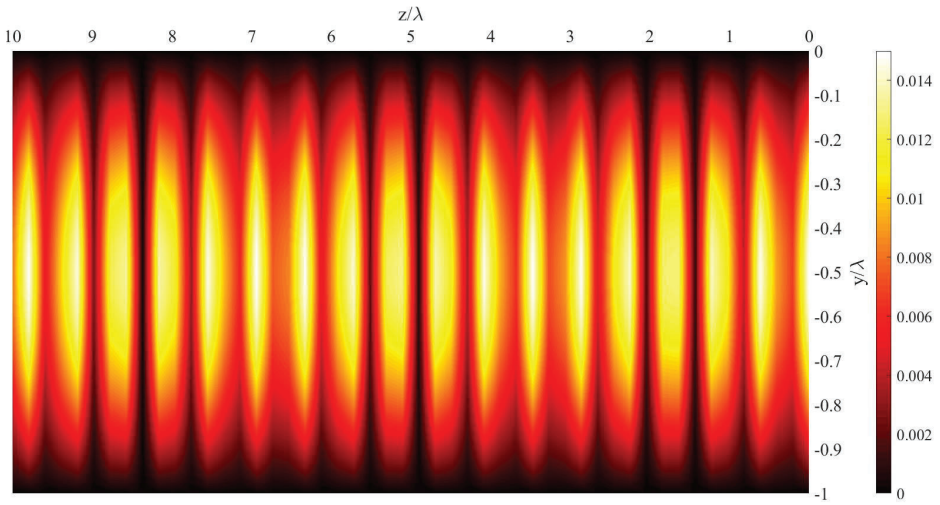

Figure 36. Magnitude of $J_z^{(e)}$ on the right-side plate of the pillar $(x = 0,\ -\lambda \leq y \leq 0,\ 10\lambda \leq z \leq 0)$ when $\theta_0 = \pi/6$, $\varphi_0 = \pi/3$, and $a = 1\lambda$.

geometry of the problem is shown in Figure 40. The 3-D electric field of the primary incident waves are given in Equation 3.5 to Equation 3.8; while the corresponding magnetic field can be found by Maxwell's equations. The exact total 3-D field is given in Equation 3.75 and Equation 3.76, which consists of standing waves in the x and $y-$direction that fill the entire space surrounding the pillars structure. There are no traveling waves or modes that propagate in any direction in this structure. The incidence angle θ_0 is given in Equation 3.81. The conditions given in Equation 3.59 and Equation 3.78 apply.

The surface current density $\underline{\mathbf{J}}^{(\mathbf{e})}$ on the truncating plane $z = 0$ ia given in Equation 3.82. If j is the number of the pillar $(j = 1, 2, 3, ...)$ in the metallic structure, then the surface current

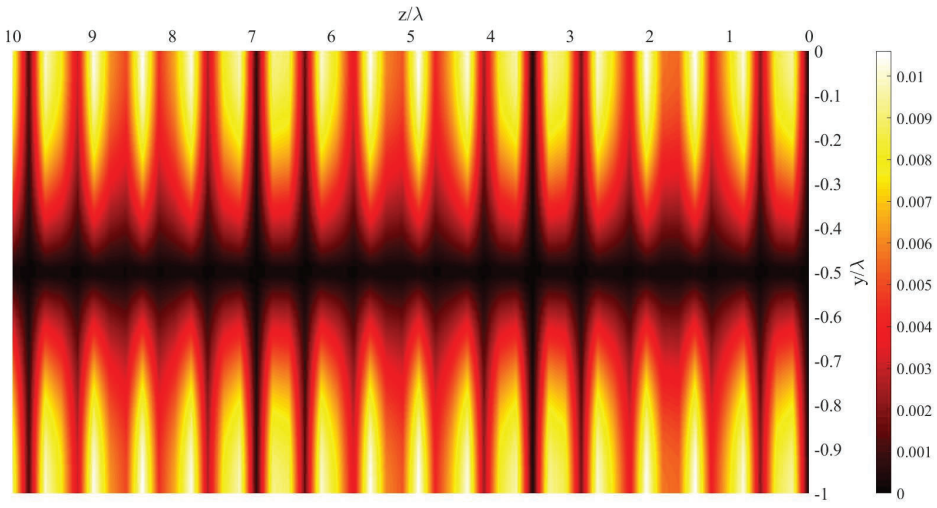

Figure 37. Magnitude of $J_y^{(h)}$ on the right-side plate of the pillar $(x = 0,\ -\lambda \leq y \leq 0,\ 10\lambda \leq z \leq 0)$ when $\theta_0 = \pi/6$, $\varphi_0 = \pi/3$, and $a = 1\lambda$.

density on the upper faces of the pillars $-ja_1 - (j-1)a_2 \leq x \leq (j-1)(-a_1 - a_2),\ y = 0$, and on the bottom faces of the pillar $-ja_1 - (j-1)a_2 \leq x \leq (j-1)(-a_1 - a_2), y = -b$, are given in Equation 3.99, Equation 3.100, respectively.

The surface current density on the right-side walls of the pillar $x = (j-1)(-a_1 - a_2),\ -b \leq y \leq 0$, is given by

$$\underline{\mathbf{J}}^{(\mathbf{e})}|_{x=0,-a_1-a_2,-2a_1-2a_2,\ldots} = \hat{x} \times \underline{\mathbf{H}}^{(\mathbf{e})} = \hat{z}8jY\eta \cos(kz\cos\theta_0)\cos\varphi_0 \sin\left(\frac{n\pi}{b}y\right). \qquad (3.107)$$

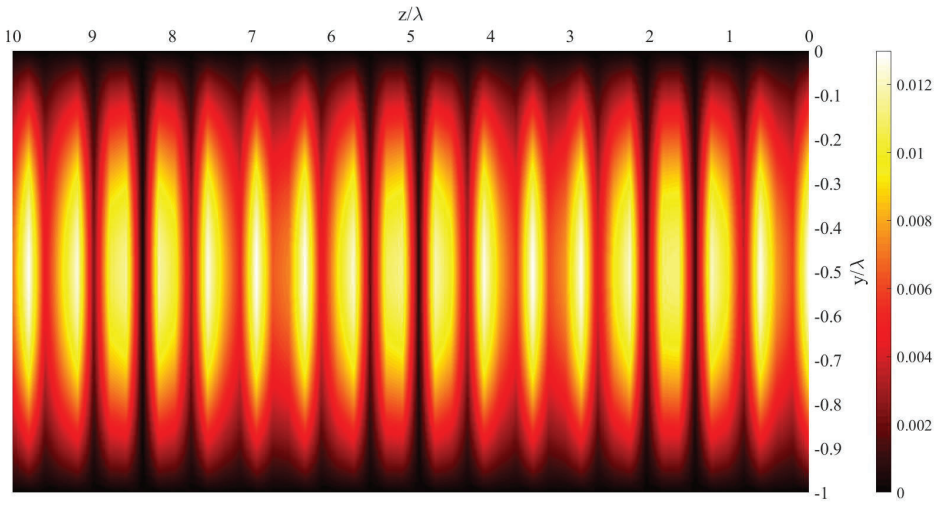

Figure 38. Magnitude of $J_z^{(h)}$ on the right-side plate of the pillar $(x = 0,\ -\lambda \leq y \leq 0,\ 10\lambda \leq z \leq 0)$ when $\theta_0 = \pi/6$, $\varphi_0 = \pi/3$, and $a = 1\lambda$.

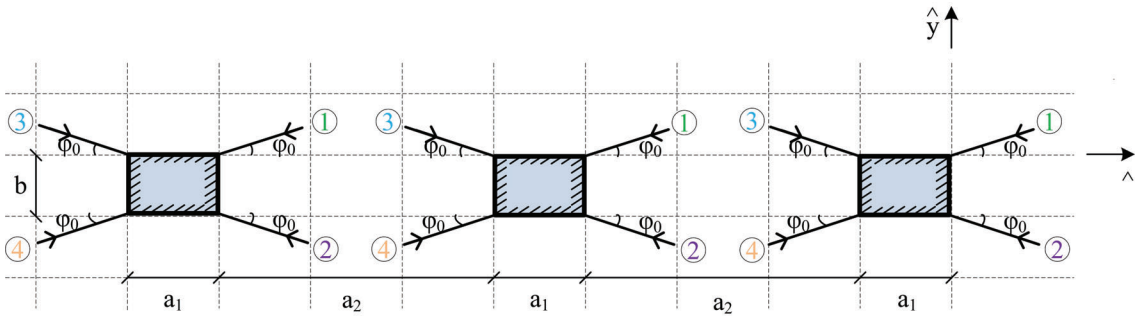

Figure 39. Two-dimensional geometry of an array of three rectangular pillars with the grid.

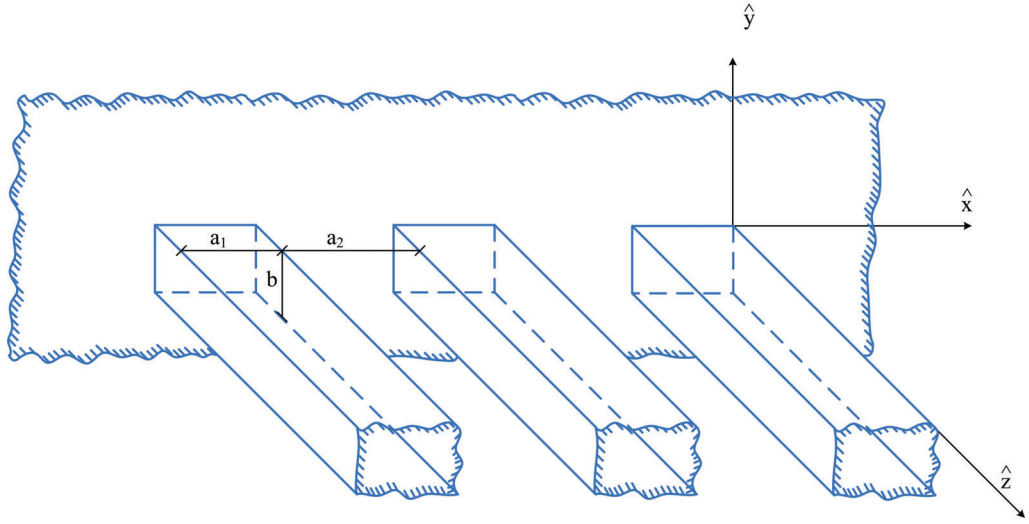

Figure 40. Three-dimensional geometry of an array of three truncated rectangular cross-section pillars.

The surface current density on the left-side walls of the pillar $x = -a_1 j - (j-1)a_2,\ -b \le y \le 0$ is given by

$$\underline{\mathbf{J}}^{(\mathbf{e})}|_{x=-a_1,-2a_1-a_2,-3a_1-2a_2,\ldots} = -\hat{x} \times \underline{\mathbf{H}}^{(\mathbf{e})} = -\hat{z}8jY\eta \cos(kz\cos\theta_0)\cos\varphi_0 \sin\left(\frac{n\pi}{b}y\right) \quad (3.108)$$

where η is given in Equation 3.54.

3.8.2 Solution to the H-polarization

The exact total 2-D magnetic field is given in Equation 2.18. It is the sum of the magnetic field of the four incident plane waves, which are given in Equation 2.14 to Equation 2.17. The related total 2-D electric field is given in Equation 2.19 and Equation 2.20. The total 3-D field

is given in Equation 3.88 and Equation 3.89 , which is found by using the general procedure in (15). The entire space surrounding the pillars is filled with standing waves without any traveling wave.

The surface current density $\underline{\mathbf{J}}^{(\mathbf{h})}$ on the truncating plane $z = 0$ ia given in Equation 3.90. The surface current density on the upper faces of the pillars $-ja_1 - (j-1)a_2 \leq x \leq (j-1)(-a_1 - a_2),\ y = 0$, and on the bottom faces of the pillar $-ja_1-(j-1)a_2 \leq x \leq (j-1)(-a_1-a_2),\ y = -b$, are given in Equation 3.103, Equation 3.104, respectively.

The surface current density on the right-side walls of the pillars $x = (j-1)(-a_1 - a_2), -b \leq y \leq 0$, is given by

$$\underline{\mathbf{J}}^{(\mathbf{h})}|_{x=0,-a_1-a_2,-2a_1-2a_2,\ldots} = \hat{x} \times \underline{\mathbf{H}}^{(\mathbf{h})} = -8jY\eta\Big[+ \hat{y}\sin\theta_0 \sin(kz\cos\theta_0)\cos\left(\frac{n\pi}{b}y\right) + \hat{z}\cos\theta_0\cos(kz\cos\theta_0)\sin\varphi_0\sin\left(\frac{n\pi}{b}y\right)\Big]. \tag{3.109}$$

The surface current density on the left-side walls of the pillars $x = -a_1 j-(j-1)a_2,\ -b \leq y \leq 0$ is given by

$$\underline{\mathbf{J}}^{(\mathbf{h})}|_{x=-a_1,-2a_1-a_2,-3a_1-2a_2,\ldots} = -\hat{x} \times \underline{\mathbf{H}}^{(\mathbf{h})} = 8jY\eta\Big[+ \hat{y}\sin\theta_0 \sin(kz\cos\theta_0)\cos\left(\frac{n\pi}{b}y\right) + \hat{z}\cos\theta_0\cos(kz\cos\theta_0)\sin\varphi_0\sin\left(\frac{n\pi}{b}y\right)\Big]. \tag{3.110}$$

3.9 Three Different Size Pillars

Figure 41 shows two-dimensional geometry of a metallic structure consists of three pillars with different size. All the horizontal dimensions (a_1, a_2, a_2) of the pillars and the horizontal separation distances (h_1, h_2) should be commensurable one to another. Also, all the vertical dimensions (b_1, b_2, b_3, b_4) of the pillars and the vertical separation distances (v_1, v_2) should be commensurable one to another, as one of the fundamental requirements to construct the grid and apply the grid method. The structure belongs to the four-quadrant structures; therefore, all the four incident plane waves of Figure 1 are required to obtain the GO solutions to the problem.

To construct the grid, all the characteristic lengths of the metallic structure need to be specified. There are five characteristic lengths in the horizontal axis, which are the horizontal dimensions of the pillars (a_1, a_2, a_3) and the horizontal separation distances (h_1, h_2). The best choice for the horizontal basic-length of the rectangles (grid's elements) a is to be equal to the smallest horizontal characteristic length in the metallic structure, thus

$$a = \min(a_1, a_2, a_3, h_1, h_2) \tag{3.111}$$

A similar rule is applied to find the best vertical basic-length of the grid's elements b, which is given by

$$b = \min(b_1, b_2, b_3, b_4, v_1, v_2). \tag{3.112}$$

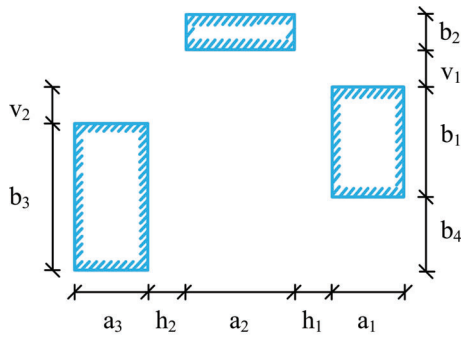

Figure 41. Two-dimensional geometry of three different size pillars structure

Based on the dimensions in Figure 41, the smallest characteristic length in the horizontal and vertical axis are h_1 and v_1; therefore, the horizontal basic-length a and the vertical basic-length b of the grid's elements equal to h_1 and v_1, respectively. The 2-D geometry of the metallic structure with the grid is shown in Figure 42. It is possible to choose values for a and b less than h_1 and v_1, respectively, but the ratio h_1/a and v_1/b should equal to an integer number. However, choosing values for a and b less than the smallest characteristic lengths in the horizontal and vertical axis, respectively, will increase the minimum frequency for which the GO solutions exist, which is not recommended practically.

Both conditions in Equation 2.11 and Equation 2.12 apply. The wavelength of the incident plane waves is given in Equation 2.25 and it should satisfy both conditions in Equation 2.27. There are m or n possible values for the incident angle φ_0, which are given in Equation 2.30 and Equation 2.31, where m and n are the integers that are used in the conditions Equation 2.11 and Equation 2.12.

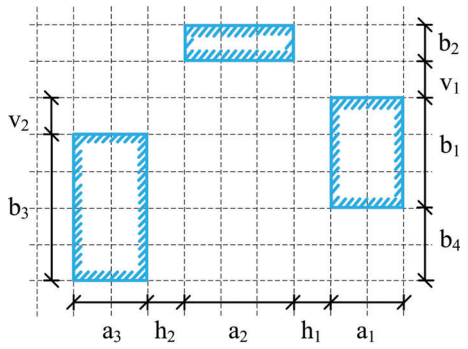

Figure 42. Two-dimensional geometry of the metallic structure with the appropriate grid.

3.9.1 Solution to the E-polarization

Based on the grid method, the total 2-D electric field equals to the sum of the electric field of the four incident plane waves, which are given in Equation 2.1 to Equation 2.4 and it is given in Equation 2.5; while the related total 2-D magnetic field is given in Equation 2.6 and Equation 2.7.

The 3-D solution is obtained by following the procedure in (15), and it given in Equation 3.75 and Equation 3.76. In the 3-D solution, the conditions in Equation 3.59 and Equation 3.78 apply, and the angle of incidence θ_0 is given in Equation 3.81. The entire space surrounding the pillars structure is filled with standing waves in the $x-$ and $y-$direction without any traveling waves.

3.9.2 Solution to the H-polarization

The total 2-D magnetic field is given in Equation 2.18, which is obtained based on the grid method. The related electric field is given in Equation 2.19 and Equation 2.20. The total 3-D solution for oblique incidence is given in Equation 3.88 and Equation 3.89. Similar to the case of E-polarization, The entire space surrounding the pillars structure is filled with standing waves in the $x-$ and $y-$direction without any traveling waves. The conditions given in Equation 3.59 and Equation 3.78 apply, and the incidence angle θ_0 is given in Equation 3.81.

The surface current density on the different faces of the pillars in the metallic structure can be obtained from $\underline{\mathbf{J}} = \hat{n} \times \underline{\mathbf{H}}$, where $\hat{n}$ is the unit normal pointing away from the metal surface.

CHAPTER 4

CONCLUSIONS AND SUGGESTIONS FOR FUTURE WORK

4.1 Conclusions

The scattering of multiple plane waves by specific metallic structures consisting of any number of metal strips either parallel or perpendicular to one another is developed in this work based on a proposed method called "Grid Method". The grid method is applied to find the possible 2-D exact GO solutions to the scattering problem under a multiple plane waves excitation for several metallic structures with strips and right-angle wedges. The solution is performed in the phasor domain. General and specific conditions for the existence of exact geometrical optics solutions are derived and discussed. The following can be concluded from the analysis and results in this work:

1. The grid method is explained in this work, which is a general procedure that has been developed for obtaining exact GO scattering solutions under incidence by four primary or imaged plane waves impinging upon a two-dimensional structure consisting of simply or multiply connected PEC strips either parallel or perpendicular to one another. From the analysis of the previous chapters, the following theorem can be stated:

   "A sufficient condition for the existence of an exact GO solution to the scattering of four primary or imaged plane waves of sufficiently high frequency by a two-dimensional structure consisting of plane PEC strips either parallel or perpendicular to one another is that

the ratio of any two characteristic dimensions in the same direction be equal to the ratio of two integer numbers".

2. The two-dimensional exact GO solutions that are obtained by employing the grid method may be extended to oblique incidence of the primary waves with respect to the $z-$axis and truncation of the structure with a PEC plane perpendicular to the $z-$axis, by following the general procedure described in (15).

3. The surface current density on the surfaces of the metallic structures were obtained. The parallel component to the intersections (edges) vanishes along the intersections (edges); while the perpendicular component is continuous across the intersections and it has a maximum value at the intersections, as it moves across the intersections to avoid charge accumulation at them and to assure the continuity of the current density across the intersection (edge) of the metal structure.

4. The solutions obtained by the grid method represent a novel canonical solutions to scattering problems.

5. The solutions may be helpful in validating complicated analytical solutions and commercially available computer solvers.

4.2 Suggestions for Future Work

As a future work expansion for this work, the following can be considered:

1. Develop a new grid structure that can be used to obtain the possible exact GO solutions to the scattering problem by radial metallic structures, such structures have several semi-infinite planes that share one edge and arrange radially with same or different angle between each two adjacent planes.

2. The grid method can be extended to Perfect Magnetic Conductors (PMC) by applying the duality principle.

CITED LITERATURE

1. Sommerfeld, A.: Mathematische theorie der diffraction. Mathematische Annalen, 47(2):317–374, Jun 1896.

2. MacDonald, H. M.: Electric waves. Cambridge University Press, 1902.

3. Carlson, J. F. and Heins, A. E.: The reflection of an electromagnetic plane wave by an infinite set of plates. i. Quarterly of Applied Mathematics, 4(4):313–329, 1947.

4. Carlson, J. F. and Heins, A. E.: The reflection of an electromagnetic plane wave by an infinite set of plates. ii. Quarterly of Applied Mathematics, 5(1):82–88, 1947.

5. Whitehead, E.: The theory of parallel-plate media for microwave lenses. Proceedings of the IEE-Part III: Radio and Communication Engineering, 98(52):133–140, 1951.

6. Heins, A. E.: The reflection of an electromagnetic plane wave by an infinite set of plates. iii. Quarterly of Applied Mathematics, 8(1):281–291, 1950.

7. Weinstein, L. A.: The theory of diffraction and the factorization method. Boulder, CO, USA, Golem Press, 1969.

8. Heins, A. E.: The radiation and transmission properties of a pair of semi-infinite parallel plates. i. Quarterly of Applied Mathematics, 6(2):157–166, 1948.

9. Heins, A. E.: The radiation and transmission properties of a pair of parallel plates. ii. Quarterly of Applied Mathematics, 6(3):215–220, 1948.

10. Noble, B.: Methods based on the Wiener-Hopf technique for the solution of partial differential equations. Belfast, Ireland: Pergamon Press, 1958.

11. Mittra, R. and Lee, S. W.: Analytical techniques in the theory of guided waves. New York, USA, The Macmillan Company, 1971.

12. Poort, M. D., Daniele, V. G., and Uslenghi, P. L.: Electromagnetic scattering by an array of parallel metallic half-planes perpendicularly truncated by a metal plane. In 2016

URSI International Symposium on Electromagnetic Theory (EMTS), pages 69–72. IEEE, 2016.

13. Poort, M. D., Daniele, V. G., and Uslenghi, P. L.: Electromagnetic scattering by an infinite array of truncated metal plates. Radio Science, 52(4):490–497, 2017.

14. Poort, M. D., Daniele, V. G., and Uslenghi, P. L.: Electromagnetic scattering by a pair of semi-infinite metal plates perpendicularly truncated by a metal ground plane. IEEE Transactions on Antennas and Propagation, 66(5):2515–2521, 2018.

15. Uslenghi, P. L. E.: Electromagnetic scattering by metallic cylinders perpendicularly truncated by a metal plane. IEEE Transactions on Antennas and Propagation, 63(5):2228–2236, 2015.

16. Lee, S. W.: Radiation from an infinite array of parallel-plate waveguides with thick walls. IEEE Transactions on Microwave Theory and Techniques, 15(6):364–371, 1967.

17. Tasinkevych, Y.: Em scattering by the parallel plate waveguide array with thick walls for oblique incidence. Journal of Electromagnetic Waves and Applications, 23(11-12):1611–1621, 2009.

18. Uslenghi, P. L. E.: Exact geometrical optics scattering by a right-angle metallic wedge illuminated by three plane waves. In Digest of the 2019 USNC-URSI National Radio Science Meeting, Boulder, CO, 2019.

19. Bowman, J. J., Senior, T. B., and Uslenghi, P. L.: Electromagnetic and acoustic scattering by simple shapes (Revised edition). New York: Hemisphere, 1987.

20. Uslenghi, P. L. E.: Geometrical optics exact solutions for two classes of dielectric wedge structures. IEEE Transactions on Antennas and Propagation, 44(1):129, 1996.

21. Uslenghi, P. L. E.: Exact solution for a penetrable wedge structure. IEEE Transactions on Antennas and Propagation, 45(1):179, 1997.

22. Uslenghi, P. L. E.: Exact geometrical optics solution for an isorefractive wedge structure. IEEE Transactions on Antennas and Propagation, 48(2):335–336, 2000.

23. Uslenghi, P. L. E.: Exact geometrical optics scattering from a tri-sector isorefractive wedge structure. IEEE Antennas and Wireless Propagation Letters, 3:94–95, 2004.

24. Uslenghi, P. L. E.: Exact geometrical optics scattering from a right-angle isorefractive wedge structure. IEEE Antennas and Wireless Propagation Letters, 3(1):127–128, 2004.

25. Uslenghi, P. L. E.: Exact geometrical optics scattering by a right-angle wedge made of double-negative material. IEEE Transactions on Antennas and Propagation, 54(8):2301–2304, 2006.

26. Uslenghi, P. L. E.: Exact geometrical optics scattering by a truncated rectangular metal trench. In 2019 Intl. Conference on Electromagnetics in Advanced Applications (ICEAA), Granada, Spain, 2019.

27. Uslenghi, P. L. E.: Exact geometrical optics scattering by a 45^o metal wedge illuminated by multiple plane waves. In 2019 URSI International Symposium on Electromagnetic Theory (EMTS), pages 1–3. IEEE, 2019.

28. Uslenghi, P. L. E.: Exact geometrical optics scattering by a class of metallic wedges under multiple plane waves illumination. In IEEE Intl. Symp. on Antennas and Propagation & USNC-URSI Radio Science Meeting, Atlanta, GA, 2019.

29. Uslenghi, P. L. E.: Exact geometrical optics scattering by a truncated metallic cylinder of rectangular cross section under multiple plane waves illumination. In 2019 Photonics and Electromagnetics Research Symposium (PIERS), Rome, Italy, 2019.

30. Uslenghi, P. L. E.: Exact geometrical optics scattering by metallic structures with sharp edges under multiple plane waves illumination. In 2019 International Conference on Microwaves, Communications, Antennas and Electronic Systems (IEEE COMCAS), Tel Aviv, Israel, 2019.

31. Al-Bahri, B. B. and Uslenghi, P. L. E.: Exact geometrical optics scattering by truncated metal gratings. In 2020 URSI GASS, Rome, Italy, 2020.

32. Uslenghi, P. L. E.: Exact geometrical optics scattering by a class of metallic wedges under multiple plane waves illumination. Radio Science Letters, 1, 2019. DOI: 10.46620/19-0005.

33. Al-Bahri, B. B. and Uslenghi, P. L. E.: Exact scattering by metal structures with strips and right-angle wedges. Radio Science Letters, 2, 2020. DOI: 10.46620/20-0022.

34. Lombardi, G. and Graglia, R. D.: Modeling junctions in sharp edge conducting structures with higher order method of moments. IEEE Transactions on Antennas and Propagation, 62(11):5723–5731, 2014.

35. Erricolo, D., Uslenghi, P. L. E., Elnour, B., and Mioc, F.: Scattering by a blade on a metallic plane. Electromagnetics, 26(1):57–71, 2006.

36. Daniele, V. and Zich, R.: The Wiener-Hopf Method in Electromagnetics. NJ, USA, IEE SciTech Publishing, 2014.

VITA (continued)

NAME: Baker Basil Al-Bahri

EDUCATION: B.S., Electronic and Communication Engineering, University of Baghdad, Iraq, 1996.

M.S., Laser Applications in Electronic and Communication Engineering, University of Baghdad, Iraq, 2001.

Ph.D., Electronic and Communication Engineering, Al-Nahrain University, Iraq, 2006.

M.S., Electrical and Computer Engineering, University of Illinois At Chicago, USA, 2016.

Ph.D., Electrical and Computer Engineering, University of Illinois At Chicago, USA, 2021.

TEACHING: From 2002 to 2013 teaching in several universities in Iraq and Oman.

PUBLICATIONS: Al-Bahri, B. B. and Uslenghi, P. L. E.: Exact geometrical optics scattering by truncated metal gratings. In 2020 URSI GASS, Rome, Italy, 2020.

Al-Bahri, B. B. and Uslenghi, P. L. E.: Exact scattering by metal structures with strips and right-angle wedges. Radio Science Letters, 2, 2020. DOI: 10.46620/20-0022.